# Integrable Deformations of Discrete Curves and Their Applications

朴, 炯基

Dissertation for the Degree of Doctor of Philosophy

# Integrable Deformations of Discrete Curves and Their Applications

Graduate School of Mathematics
Kyushu University

Hyeongki Park

Supervisor : Professor Kenji Kajiwara
Submission date : 23/12/2020

# Contents

# 1 Introduction

It is well-known that differential geometry is closely related to the theory of the integrable systems, and various integrable equations arise as compatibility conditions of the geometric objects such as the curves and surfaces. A typical example is the pseudospherical surfaces described by the sine-Gordon equation under the Chebyshev net parametrization. For more information on such connections we refer to a monograph [9] by Rogers and Schief. On the other hand, in the theory of the connections between differential geometry and the integrable systems, the discretizations of this theory preserving the underlying integrable structure have been actively studied by many researchers under the name of the *discrete differential geometry* [10].

In this thesis, we particularly interested in the relation between deformations of curves and integrable systems, which has been first pointed out by Hasimoto [39], and then studied further by Lamb and Goldstein-Petrich [12,51]. In these researches it has been clarified that certain deformations of curves in the Euclidean geometry are governed by the AKNS hierarchy. Then, in the development of the discrete differential geometry, the discretizations of these theories have been studied in [1, 8, 13–19, 35], which mean to construct the frameworks of discrete plane and space curves governed by the semi-discrete or discrete integrable systems. Besides the Euclidean geometry, deformations of smooth and discrete curves in various Klein geometries have been studied in [6–8, 20–23].

The purpose of this thesis is to investigate deformations of smooth and discrete curves, which are described by continuous and semi-discrete integrable equations, in the Euclidean geometry and the centroaffine geometry which is one of Klein geometries, and present an relationship between the integrable deformation of discrete curves and linkage mechanisms.

In the first part of this thesis, we consider a certain deformation of smooth plane curves in the centroaffine geometry, which is governed by the *defocusing modified Korteweg-de Vries equation* (mKdV equation). Then we construct a framework of discrete plane curves in the centroaffine geometry (discrete centroaffine plane curves), and present a particular deformation of discrete centroaffine plane curves governed by the *Lotka-Volterra equation*. On the other hand, it is known that the KdV equation and its semi-discrete analog describe the integrable deformations of smooth and discrete plane curves in the equicentroaffine geometry [5–8], and a solution to the KdV equation can be constructed from a solution to the (defocusing) mKdV equation by the *Miura transformation* [42]. We investigate the correspondences between deformations of centroaffine and equicentroaffine plane curves by using the Miura transformation.

In the next part of this thesis, we present a mathematical model of a special class of linkages, which is called the *Kaleidocycles*, by using the theory of discrete space curves. A linkage is a mechanical system consisting of rigid bodies joined together by joints. They are used to transform one motion to another as in the famous Watt parallel motion and a lot of examples are found in engineering as well as in natural creatures [31]. In particular, we focus on linkages consisting of hinge joints in this thesis.

Meanwhile, we also consider continuous deformations of discrete space curves in the Euclidean geometry, which are governed by the semi-discrete mKdV and the semi-discrete sine-Gordon equations. Many researchers, working on the discrete differential geometry, have studied various continuous deformations of the discrete space curves in [1, 35, 40, 60, 62]. We present how to identify hinged linkages by using discrete space curves, and investigate particular configuration spaces of hinged linkages which are governed by the semi-discrete mKdV and the semi-discrete sine-Gordon equations.

In the last part of this thesis, we introduce a figure called the *spherical Kaleidocycle*, which is defined on the standard unit 3-sphere in $\mathbb{R}^4$. It has the similar shape with the Kaleidocycles if we see it in $\mathbb{R}^3$ via the stereographic projection. Moreover, a particular deformation of it exhibits the turning-over motion, which is reminiscent of the motion of Kaleidocycles. We present an algorithm to construct spherical Kaleidocycles and visualize them.

This thesis is organized as follows. In Chapter 2, we present frameworks of plane curves in the centroaffine geometry, and consider continuous deformations of smooth and discrete centroaffine plane curves governed by the defocusing mKdV and Lotka-Volterra equations, respectively. In Chapter 3, we review the deformation of smooth plane curves in the equicentroaffine geometry described by the KdV equation, and its semi-discrete analog based on [5, 8]. Then we construct correspondences between continuous deformations of smooth and discrete plane curves in the centroaffine geometry and the equicentroaffne geometry in Chapter 4. In Chapter 5, first in Section 5.1 and 5.2, we set up a mathematical model of linkages. Next in Section 5.3–5.5, We formulate Kaleidocycles by using discrete space curves and investigate the relationship between the motion of Kaleidocycles and deformations of discrete space curves governed by the semi-discrete mKdV and semi-discrete sine-Gordon equations. Then in Section 5.6–5.8, we introduce some properties and numerical observations about motions of Kaleidocycles. Finally in Chapter 6, we prepare some basic theories of the standard unit 3-sphere and the Clifford torus, and then we construct the spherical Kaleidocycles.

# Acknowledgements

Throughout completing of this dissertation I have received a great deal of support and assistance.

Foremost, I would first like to express my sincere gratitude to my supervisor Prof. Kenji Kajiwara for the continuous support of my research. His guidance helped me in all the time of research and writing of this thesis. Moreover, he and his family supported me not only for my work, but also for my private life in Japan. Without his supervision, I would not have completed my challenge.

Besides my supervisor, I would like to thank the rest of examiners, Prof. Junichi Inoguchi, Prof. Nozomu Matsuura and Prof. Konrad Polthier, for their encouragement and enlightening comments.

My sincere thanks also go to all of collaborators for studies in this thesis. The contents in Chapter 2–4 are joint works with Prof. Kenji Kajiwara, Prof. Takashi Kurose and Prof. Nozomu Matsuura, and the contents of Chapter 5 are joint works with Prof. Shizuo Kaji and Prof. Kenji Kajiwara. Also the contents of Chapter 6 are joint works with Prof. Konrad Polthier.

This work would not have been possible without the financial support from the "Leading Program in Mathematics for Key Technologies" of Graduate School of Mathematics, Kyushu University, and the "Korea Scholarship Foundation". Especially, I would like to thank all of members of "Leading Program in Mathematics for Key Technologies". They are my good friends, mates of study and supporters of my life in Japan. Without their support, I may not have finished my study so smoothly.

Finally, but definitely not the least, I am extremely grateful to my family, Nogul Park, Okhee Shin, Hyeonjung Park and Hyeonkyu Lee, for their permanent love, encouraging and sacrifices. I dedicate this thesis to them.

# 2 Integrable deformation of plane curves in the centroaffine geometry

In this chapter, we present a framework of the smooth/discrete curve theories in the centroaffine geometry. Also, we investigate particular curve deformations that are described by the defocusing mKdV and the Lotka-Volterra equations.

## 2.1 Defocusing mKdV flow on smooth centroaffine plane curves

In this section, we investigate a continuous curve deformation in the centroaffine geometry based on [2,3], that is described by the defocusing mKdV equation. The defocusing mKdV equation has diffenrent properties from that of the focusing one, since it does not have a traveling wave solution under the rapidly decreasing boundary condition. It should be noted that Chou and Qu formulated in [4] a curve deformation described by the defocusing mKdV equation, however, while their formulation depends on quantities of the Euclidean geometry, ours is independent of those. We introduce an invariant parameter for curves, which is a centroaffine analogue of the arclength parameter, and then formulate the defocusing mKdV flow as the simplest deformation that preserves the centroaffine arclength. In this geometry, we are interested in the invariants of the *centroaffine transformation*:

**Definition 2.1 (centroaffine transformation)** *Let $\phi : \mathbb{R}^n \to \mathbb{R}^n$ be a linear transformation. Then $\phi$ is called the centroaffine transformation if it is expressed, for any $x \in \mathbb{R}^n$, as*

$$\phi(x) = Ax, \quad A \in \mathrm{GL}(n), \tag{2.1}$$

*where $\mathrm{GL}(n)$ is the general linear group.*

Since the arclength is not an invariant for the centroaffine transformation, we need to look for a different invariant value. We simply regard $\mathbb{R}^2$ as a vector space, and consider a plane curve $\gamma(\xi) : I \subset \mathbb{R} \to \mathbb{R}^2$ which is parametrized by an arbitrary parameter $\xi$. Also we introduce a frame $\Phi(\xi) = \left[\gamma(\xi), \gamma_\xi(\xi)\right]$, where the subscript indicates differentiation with respect to the designated parameter. We assume that $\det \Phi(\xi) \neq 0$. Then, for a nonzero real number $\lambda$, we reparametrize $\gamma = \gamma(\xi)$ for a parameter $x$ so as to be

$$\frac{\det[\gamma_x, \gamma_{xx}]}{\det[\gamma, \gamma_x]} = \lambda. \tag{2.2}$$

In fact, we can look for $x = x(\xi)$ as

$$\begin{aligned} \det\left[\gamma_\xi, \gamma_{\xi\xi}\right] &= \left(x_\xi\right)^3 \det\left[\gamma_x, \gamma_{xx}\right] \\ &= \left(x_\xi\right)^3 \lambda \det\left[\gamma, \gamma_x\right] \\ &= \left(x_\xi\right)^2 \lambda \det\left[\gamma, \gamma_\xi\right], \end{aligned} \tag{2.3}$$

which implies that

$$x(\xi) = \int_{\xi_0}^{\xi} \left( \frac{\det\left[\gamma_\xi, \gamma_{\xi\xi}\right]}{\lambda \det\left[\gamma, \gamma_\xi\right]} \right)^{1/2} d\xi. \tag{2.4}$$

In order for (2.4) to define a reparametrization $\xi \mapsto x$, we shall assume that the given curve $\gamma$ satisfies the condition $\det\left[\gamma_\xi, \gamma_{\xi\xi}\right] \neq 0$. We summarize the above discussion as follows.

**Definition 2.2 (centroaffine plane curve)**

1. *Let $\gamma(\xi) : I \subset \mathbb{R} \to \mathbb{R}^2$ be a parametrized plane curve in the centroaffine geometry, where $\xi$ is an arbitrary parameter. We call $\gamma(\xi)$ a centroaffine plane curve if $\gamma(\xi)$ satisfies $\det\left[\gamma(\xi), \gamma_\xi(\xi)\right] \neq 0$ for all $\xi$.*

2. *Let $\gamma(\xi)$ be a centroaffine plane curve. We call $\gamma(\xi)$ is regular if it satisfies $\det\left[\gamma_\xi(\xi),\ \gamma_{\xi\xi}(\xi)\right] \neq 0$ for all $\xi$.*

3. *Let $\gamma(\xi)$ be a regular centroaffine plane curve. Then, for a nonzero real number $\lambda$, $\gamma(\xi)$ can be reparametrized by the parameter $x$ in such a way that in (2.2). We call the parameter $x$ the centroaffine arclength parameter, and it can be derived from $\xi$ as (2.4).*

Let $\gamma(x)$ be a centroaffine arclength parametrized centroaffine plane curve. Then, there exists a function $\kappa = \kappa(x)$ satisfies

$$\gamma_{xx} = -\lambda\gamma + \kappa\gamma_x. \tag{2.5}$$

We call the function $\kappa$ the *centroaffine curvature*. It is easy to verify that $\kappa$ also can be expressed as

$$\kappa = \frac{\det\left[\gamma, \gamma_{xx}\right]}{\det\left[\gamma, \gamma_x\right]}. \tag{2.6}$$

**Proposition 2.3** *The centroaffine arclength and the centroaffine curvature are invariant under the centroaffine transformation.*

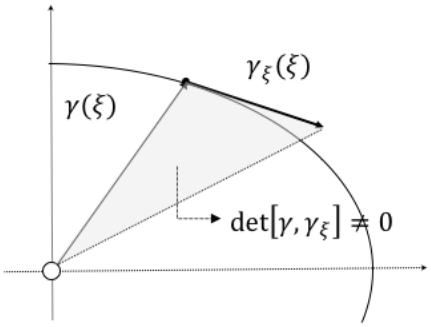


Figure 1: Centroaffine plane curve.

*Proof.* Let $\gamma = \gamma(\xi)$ be a regular centroaffine plane curve parametrized by an arbitrary parameter $\xi$. For any $A \in \mathrm{GL}(2)$, we define a curve $\gamma^A = \gamma^A(\xi)$ by $\gamma^A = A\gamma$. Then, $\gamma^A$ is also a regular centroaffine plane curve since

$$\det[\gamma^A, \gamma^A_\xi] = \det[A\gamma, A\gamma_\xi] = (\det A)^2 \det[\gamma, \gamma_\xi] \neq 0, \tag{2.7}$$

$$\det[\gamma^A_\xi, \gamma^A_{\xi\xi}] = \det[A\gamma_\xi, A\gamma_{\xi\xi}] = (\det A)^2 \det[\gamma_\xi, \gamma_{\xi\xi}] \neq 0. \tag{2.8}$$

The parameter $x^A = x^A(\xi)$ characterized by

$$\frac{\det\left[\gamma^A_{x^A}, \gamma^A_{x^A x^A}\right]}{\det\left[\gamma^A, \gamma^A_{x^A}\right]} = \lambda, \tag{2.9}$$

satisfies

$$\begin{aligned} x^A &= \int_{\xi_0}^{\xi} \left( \frac{\det\left[\gamma^A_\xi, \gamma^A_{\xi\xi}\right]}{\lambda \det\left[\gamma^A, \gamma^A_\xi\right]} \right)^{1/2} d\xi \\ &= \int_{\xi_0}^{\xi} \left( \frac{\det\left[A\gamma_\xi, A\gamma_{\xi\xi}\right]}{\lambda \det\left[A\gamma, A\gamma_\xi\right]} \right)^{1/2} d\xi \\ &= \int_{\xi_0}^{\xi} \left( \frac{\det\left[\gamma_\xi, \gamma_{\xi\xi}\right]}{\lambda \det\left[\gamma, \gamma_\xi\right]} \right)^{1/2} d\xi = x. \end{aligned} \tag{2.10}$$

Similarly, the centroaffine curvature $\kappa^A$ of $\gamma^A$ satisfies by (2.10)

$$\kappa^A = \frac{\det\left[\gamma^A, \gamma^A_{x^A x^A}\right]}{\det\left[\gamma^A, \gamma^A_{x^A}\right]} = \frac{\det\left[\gamma^A, \gamma^A_{xx}\right]}{\det[\gamma^A, \gamma^A_x]} = \frac{\det[A\gamma, A\gamma_{xx}]}{\det[A\gamma, A\gamma_x]} = \frac{\det[\gamma, \gamma_{xx}]}{\det[\gamma, \gamma_x]} = \kappa, \tag{2.11}$$

which prove the proposition. □

Then introducuing the frame $\Phi : \mathbb{R} \to \mathrm{GL}(2)$ given by $\Phi(x) = [\gamma, \gamma_x]$, equation (2.5) is rewritten in terms of $\Phi = \Phi(x)$ as

$$\Phi_x = \Phi L, \quad L = \begin{bmatrix} 0 & -\lambda \\ 1 & \kappa \end{bmatrix}. \tag{2.12}$$

We call it the Frenet formula of the centroaffine plane curves.

**Example 2.4** *Let us consider the special case where $\kappa = 0$. Solving (2.5), we obtain an ellipse or a hyperbola*

$$\gamma = \begin{cases} \cos\left(\sqrt{\lambda}\, x\right) e_1 + \sin\left(\sqrt{\lambda}\, x\right) e_2 & \lambda > 0 \\ \cosh\left(\sqrt{-\lambda}\, x\right) e_1 + \sinh\left(\sqrt{-\lambda}\, x\right) e_2 & \lambda < 0, \end{cases}$$

*where $e_1$ and $e_2$ are linearly independent constant vectors. We remark that straight lines are excluded from the curve theory in the centroaffine geometry, because they are not regular.*

Now we consider a family of regular centroaffine plane curves $\gamma = \gamma(x,t)$. where $x$ is the centroaffine arclength parameter at each time $t$. We define two functions

$$\lambda(t) = \frac{\det[\gamma_x, \gamma_{xx}]}{\det[\gamma, \gamma_x]}, \quad \kappa(x,t) = \frac{\det[\gamma, \gamma_{xx}]}{\det[\gamma, \gamma_x]} \tag{2.13}$$

and a deformation of the curves by

$$\gamma_t = 2\lambda\kappa\gamma + \left(\kappa_x - \frac{\kappa^2}{2} - 4\lambda\right)\gamma_x. \tag{2.14}$$

Then we have the following.

**Theorem 2.5 (defocusing mKdV flow on centroaffine plane curves [3])** *Let $\gamma = \gamma(x,t)$ be a regular centroaffine plane curve, which is deformed according to the formula (2.14). Then we have:*

1. *The frame $\Phi = \Phi(x,t)$ satisfies*

$$\Phi_t = \Phi M, \quad M = \begin{bmatrix} 2\lambda\kappa & \lambda\left(\kappa_x + \frac{1}{2}\kappa^2\right) + 4\lambda^2 \\ \kappa_x - \frac{1}{2}\kappa^2 - 4\lambda & \kappa_{xx} - \frac{1}{2}\kappa^3 - 2\lambda\kappa \end{bmatrix}. \tag{2.15}$$

2. *$\lambda$ does not depend on $t$.*

3. *The centroaffine curvature $\kappa$ satisfies the defocusing mKdV equation:*

$$\kappa_t = \kappa_{xxx} - \frac{3}{2}\kappa^2\kappa_x. \tag{2.16}$$

*Proof.* We note that (2.5) and (2.14) are rewritten, in terms of the frame $\Phi$, as

$$\gamma_{xx} = \Phi \begin{bmatrix} -\lambda \\ \kappa \end{bmatrix}, \tag{2.17}$$

$$\gamma_t = \Phi \begin{bmatrix} 2\lambda\kappa \\ \kappa_x - \frac{\kappa^2}{2} - 4\lambda \end{bmatrix}, \tag{2.18}$$

respectively. Then, differentiating (2.18) with respect to $x$, we have from (2.12)

$$\begin{aligned} \gamma_{tx} &= \Phi_x \begin{bmatrix} -2\lambda\kappa \\ \kappa_x - \frac{1}{2}\kappa^2 - 4\lambda \end{bmatrix} + \Phi \begin{bmatrix} -2\lambda\kappa_x \\ \kappa_{xx} - \kappa\kappa_x \end{bmatrix} \\ &= \Phi \left( \begin{bmatrix} 0 & -\lambda \\ 1 & \kappa \end{bmatrix} \begin{bmatrix} -2\lambda\kappa \\ \kappa_x - \frac{1}{2}\kappa^2 - 4\lambda \end{bmatrix} + \begin{bmatrix} -2\lambda\kappa_x \\ \kappa_{xx} - \kappa\kappa_x \end{bmatrix} \right) \\ &= \Phi \begin{bmatrix} \frac{1}{2}\lambda\kappa^2 + 4\lambda^2 + \lambda\kappa_x \\ \kappa_{xx} - \frac{1}{2}\kappa^3 - 2\lambda\kappa \end{bmatrix}, \end{aligned} \tag{2.19}$$

which immediately yields (2.15). Also, differentiating (2.19) with respect to $x$ again, we get

$$\begin{aligned} \gamma_{txx} &= \Phi_x \begin{bmatrix} \frac{1}{2}\lambda\kappa^2 + 4\lambda^2 + \lambda\kappa_x \\ \kappa_{xx} - \frac{1}{2}\kappa^3 - 2\lambda\kappa \end{bmatrix} + \Phi \begin{bmatrix} \lambda\kappa\kappa_x + \lambda\kappa_{xx} \\ \kappa_{xxx} - \frac{3}{2}\kappa^2\kappa_x - 2\lambda\kappa_x \end{bmatrix} \\ &= \Phi \left( \begin{bmatrix} 0 & -\lambda \\ 1 & \kappa \end{bmatrix} \begin{bmatrix} \frac{1}{2}\lambda\kappa^2 + 4\lambda^2 + \lambda\kappa_x \\ \kappa_{xx} - \frac{1}{2}\kappa^3 - 2\lambda\kappa \end{bmatrix} + \begin{bmatrix} \lambda\kappa\kappa_x + \lambda\kappa_{xx} \\ \kappa_{xxx} - \frac{3}{2}\kappa^2\kappa_x - 2\lambda\kappa_x \end{bmatrix} \right) \\ &= \Phi \begin{bmatrix} \frac{1}{2}\lambda\kappa^3 + 2\lambda^2\kappa + \lambda\kappa\kappa_x \\ \kappa_{xxx} + \kappa\kappa_{xx} - \frac{3}{2}\kappa^2\kappa_x - \lambda\kappa_x - \frac{1}{2}\kappa^4 - \frac{3}{2}\lambda\kappa^2 + 4\lambda^2 \end{bmatrix}. \end{aligned} \tag{2.20}$$

Now we verify that $\lambda$ does not depend on $t$. By differentiating (2.2) with respect to $t$, we have

$$\lambda_t = \frac{1}{(\det[\gamma, \gamma_x])^2} \left( \det[\gamma, \gamma_x] \frac{\partial}{\partial t} \det[\gamma_x, \gamma_{xx}] - \det[\gamma_x, \gamma_{xx}] \frac{\partial}{\partial t} \det[\gamma, \gamma_x] \right). \tag{2.21}$$

Then it is easy to verify that the right hand side of the (2.21) vanishes by (2.19) and (2.20), and it implies $\lambda_t = 0$. Namely, $\lambda$ does not depend on $t$. Finally we consider the compatibility condition of the Frenet formula (2.5) and the deformation

equation (2.14). Differentiating (2.17) with respect to $t$, we have

$$\begin{aligned}\gamma_{xxt} &= \Phi_t \begin{bmatrix} -\lambda \\ \kappa \end{bmatrix} + \Phi \begin{bmatrix} -\lambda_t \\ \kappa_t \end{bmatrix} \\ &= \Phi \left( \begin{bmatrix} 2\lambda\kappa & \lambda\left(\kappa_x + \frac{1}{2}\kappa^2\right) + 4\lambda^2 \\ \kappa_x - \frac{1}{2}\kappa^2 - 4\lambda & \kappa_{xx} - \frac{1}{2}\kappa^3 - 2\lambda\kappa \end{bmatrix} \begin{bmatrix} -\lambda \\ \kappa \end{bmatrix} + \begin{bmatrix} -\lambda_t \\ \kappa_t \end{bmatrix} \right) \\ &= \Phi \begin{bmatrix} \lambda\kappa\kappa_x + 2\lambda^2\kappa + \frac{1}{2}\lambda\kappa^3 - \lambda_t \\ \kappa\kappa_{xx} - \lambda\kappa_x - \frac{1}{2}\kappa^4 - \frac{3}{2}\lambda\kappa^2 + 4\lambda^2 + \kappa_t \end{bmatrix}. \end{aligned} \tag{2.22}$$

Then, by the compatibility condition $\gamma_{txx} = \gamma_{xxt}$, namely, comparing (2.20) with (2.22), we get from $\lambda_t = 0$

$$\kappa_t = \kappa_{xxx} - \frac{3}{2}\kappa^2\kappa_x,$$

which is the defocusing mKdV equation. □

## 2.2 Lotka-Volterra flow on discrete centroaffine plane curves

In this section, we construct a discrete analogue of the plane curve theory in the centroaffine geometry, and we present a particular deformation of discrete centroaffine plane curves which is governed by the Lotka-Volterra equation.

Consider a map $\gamma : \mathbb{Z} \to \mathbb{R}^2$, $n \mapsto \gamma_n$. We call $\gamma_n$ a discrete plane curve if any three consecutive points $\gamma_n$, $\gamma_{n+1}$ and $\gamma_{n+2}$ are not collinear. We define the discrete centroaffine plane curve in the similar way to the smooth case as follows.

**Definition 2.6 (discrete centroaffine plane curve)** *Let $\gamma : \mathbb{Z} \to \mathbb{R}^2$, $n \mapsto \gamma_n$ be a discrete plane curve in the centroaffine geometry. We call $\gamma_n$ a discrete centroaffine plane curve if $\gamma_n$ satisfies* $\det[\gamma_n, \gamma_{n+1}] \neq 0$.

Let $\gamma_n$ be a discrete centroaffine plane curve. We define the tangent vector $T_n$ and the second divided difference $\Delta T_n$ of $\gamma_n$ by

$$T_n = \frac{\gamma_{n+1} - \gamma_n}{\varepsilon_n}, \quad \Delta T_n = \frac{2}{\varepsilon_n + \varepsilon_{n-1}} (T_n - T_{n-1}), \tag{2.23}$$

respectively. Here $\varepsilon_n$ is determined as $\gamma_n$ satisfies

$$\lambda_n = \frac{\det[T_n, \Delta T_n]}{\det[\gamma_n, T_n]}, \tag{2.24}$$

for an arbitrary real value function $\lambda : \mathbb{Z} \to \mathbb{R}$. Then putting a function $\kappa_n$ as

$$\kappa_n = \frac{\det[\gamma_n, \Delta T_n]}{\det[\gamma_n, T_n]}, \tag{2.25}$$

we have

$$\Delta T_n = -\lambda_n \gamma_n + \kappa_n T_n, \tag{2.26}$$

which is discrete analogue of the Frenet equation of centroaffine plane curves (2.5). Introducing the frame $\Phi_n = [\gamma_n, T_n]$, the Frenet equation (2.26) is rewritten in terms of $\Phi_n$ as

$$\Phi_{n+1} = \Phi_n L_n, \quad L_n = \begin{bmatrix} 1 & v_n \\ \varepsilon_n & w_n \end{bmatrix}, \tag{2.27}$$

where $v_n$ and $w_n$ are given by

$$v_n = \frac{-(\varepsilon_{n+1} + \varepsilon_n)\lambda_{n+1}}{2 - (\varepsilon_{n+1} + \varepsilon_n)\kappa_{n+1}}, \quad w_n = \frac{2 - \varepsilon_n(\varepsilon_{n+1} + \varepsilon_n)\lambda_{n+1}}{2 - (\varepsilon_{n+1} + \varepsilon_n)\kappa_{n+1}}. \tag{2.28}$$

We note that $v_n$ and $w_n$ satisfy the following equations:

$$\frac{w_n}{v_n} = \varepsilon_n - \frac{2}{(\varepsilon_{n+1} + \varepsilon_n)\lambda_{n+1}}, \quad \varepsilon_n v_n - w_n = -\frac{2}{2 - (\varepsilon_{n+1} + \varepsilon_n)\kappa_{n+1}}. \tag{2.29}$$

Now we consider a family of discrete centroaffine plane curves $\gamma_n(t)$ with $t \in \mathbb{R}$, and define $\varepsilon_n(t)$, $\kappa_n(t)$ and $\lambda_n(t)$ as given in above discussion. We assume that $\varepsilon = \varepsilon_n(t)$ does not depend on both of $n$ and $t$. One way that we describe a motion of discrete curves is to put functions $f_n(t)$ and $g_n(t)$ as following:

$$\frac{d}{dt}\gamma_n(t) = f_n(t)\gamma_n(t) + g_n(t)T_n(t). \tag{2.30}$$

For simplicity, we denote differentiation with respect to $t$ by dot above the designated function. Then noticing that the deformation of discrete centroaffine plane curves (2.30) is rewritten in terms of $\Phi_n = \Phi_n(t)$ as

$$\dot{\gamma}_n = \Phi_n \begin{bmatrix} f_n \\ g_n \end{bmatrix}, \tag{2.31}$$

we have from (2.27) and (2.30)

$$\begin{aligned} \dot{T}_n &= \frac{1}{\varepsilon}(\dot{\gamma}_{n+1} - \dot{\gamma}_n) \\ &= \frac{1}{\varepsilon}\left(\Phi_n \begin{bmatrix} 1 & v_n \\ \varepsilon & w_n \end{bmatrix} \begin{bmatrix} f_{n+1} \\ g_{n+1} \end{bmatrix} - \Phi_n \begin{bmatrix} f_n \\ g_n \end{bmatrix}\right) \\ &= \frac{1}{\varepsilon}\Phi_n \begin{bmatrix} f_{n+1} - f_n + v_n g_{n+1} \\ \varepsilon f_{n+1} + w_n g_{n+1} - g_n \end{bmatrix}. \end{aligned} \tag{2.32}$$

Thus a deformation of discrete centroaffine plane curves given in (2.30) is rewritten in terms of $\Phi_n$ as

$$\dot{\Phi}_n = \Phi_n M_n, \quad M_n = \begin{bmatrix} f_n & \alpha_n \\ g_n & \beta_n \end{bmatrix}, \tag{2.33}$$

where $\alpha_n = \alpha_n(t)$ and $\beta_n = \beta_n(t)$ are given by

$$\alpha_n = \frac{f_{n+1} - f_n + v_n g_{n+1}}{\varepsilon}, \quad \beta_n = f_{n+1} + \frac{w_n g_{n+1} - g_n}{\varepsilon} \tag{2.34}$$

Then the compatibility condition of the difference equation (2.27) and the differential equation (2.33), namely, $\dot{L}_n = L_n M_{n+1} - M_n L_n$, yields

$$\dot{v}_n = (\beta_{n+1} - f_n)\, v_n - \alpha_n w_n + \alpha_{n+1}, \tag{2.35}$$

$$\dot{w}_n = -g_n v_n + (\beta_{n+1} - \beta_n)\, w_n + \varepsilon \alpha_{n+1}. \tag{2.36}$$

We also have from (2.35) and (2.36)

$$\begin{aligned} \varepsilon \dot{v}_n - \dot{w}_n &= (\varepsilon(\beta_{n+1} - f_n) + g_n)\, v_n - (\varepsilon \alpha_n + \beta_{n+1} - \beta_n)\, w_n \\ &= (\varepsilon(\beta_{n+1} - f_n) + g_n)\, v_n - (f_{n+1} - f_n + v_n g_{n+1} + \beta_{n+1} - \beta_n)\, w_n \\ &= (\varepsilon(\beta_{n+1} - f_n) + g_n - g_{n+1} w_n)\, v_n - (f_{n+1} - f_n + \beta_{n+1} - \beta_n)\, w_n \\ &= \varepsilon(f_{n+1} - f_n + \beta_{n+1} - \beta_n)\, v_n - (f_{n+1} - f_n + \beta_{n+1} - \beta_n)\, w_n, \end{aligned}$$

which yields

$$\frac{\varepsilon \dot{v}_n - \dot{w}_n}{\varepsilon v_n - w_n} = f_{n+1} - f_n + \beta_{n+1} - \beta_n. \tag{2.37}$$

Then we have the following.

**Theorem 2.7 (Lotka-Volterra flow on discrete centroaffine plane curves)** *Let $\gamma_n = \gamma_n(t)$ be a discrete cetroaffine plane curve, which is deformed by a formula (2.30) with*

$$f_n = k\left(v_{n-1} - \frac{1}{2\varepsilon}\right), \quad g_n = -k, \tag{2.38}$$

*where $k$ is an arbitrary constant. We assume that $\varepsilon$ does not depend on both of $n$ and $t$, and put $\lambda_n = \lambda = \varepsilon^{-2}$. Then we have:*

1. *The frame $\Phi_n = \Phi_n(t)$ satisfies*

$$\Phi_{n+1} = \Phi_n L_n, \quad L_n = \begin{bmatrix} 1 & v_n \\ \varepsilon & 0 \end{bmatrix}, \tag{2.39}$$

$$\frac{d\Phi_n}{dt} = \Phi_n M_n, \quad M_n = \frac{k}{\varepsilon}\begin{bmatrix} \varepsilon v_{n-1} - \frac{1}{2} & -v_{n-1} \\ -v_{n-1} & \varepsilon v_n + \frac{1}{2} \end{bmatrix}. \tag{2.40}$$

2. $\lambda$ *does not depend on* $t$.

3. $v_n = v_n(t)$ *satisfies the Lotka-Volterra equation:*

$$\frac{dv_n}{dt} = kv_n\left(v_{n+1} - v_{n-1}\right). \tag{2.41}$$

*Proof.* The second statement is trivial by assumption, and we immediately get $\mu_n = 0$ from (2.28) by $\lambda = \varepsilon^{-2}$, which yields (2.39). Also substituting (2.38) into (2.34), we have

$$\alpha_n = -\frac{kv_{n-1}}{\varepsilon}, \quad \beta_n = k\left(v_{n-1} + \frac{1}{2\varepsilon}\right), \tag{2.42}$$

which imply (2.40). Then the compatibility condition (2.37) is rewritten from (2.38) and (2.42) as

$$\frac{dv_n}{dt} = kv_n\left(v_{n+1} - v_{n-1}\right), \tag{2.43}$$

which is the Lotka-Volterra equation. □

# 3 Integrable deformation of plane curves in the equicentroaffine geometry

It is known that plane curves in the equicentroaffine geometry are governed by the KdV equation [5–7]. Moreover, a discretization of the curve motion has been constructed [5, 8]. In this chapter, we briefly review these results so that we construct relevances between the KdV flows on equicentroaffne plane curves and the defocusing mKdV/Lotka-Volterra flows on centroaffine plane curves, in the after section.

## 3.1 KdV flow on smooth equicentroaffine plane curves

In this section, we review the KdV flow on smooth equicentroaffine plane curves based on [5–7].

Let $\Gamma(\xi) : I \subset \mathbb{R} \to \mathbb{R}^2$ be a parametrized plane curve in the equicentroaffine plane, where $\xi$ is an arbitrary parameter. The curve $\Gamma(\xi)$ is called the *equicentroaffine plane curve* if $\Gamma(\xi)$ satisfies $\det[\Gamma, \Gamma_\xi] \neq 0$ for all $\xi$. Also, If $\Gamma(\xi)$ is an equicentroaffine plane curve, then $\Gamma(\xi)$ can be reparametrized by the parameter $x$ in such a way that $\det[\Gamma, \Gamma_x] = 1$. We call the parameter $x$ the *equicentroaffine arclength parameter*. Then, there exists the function $u = u(x)$ such that

$$\Gamma_{xx} = -u\Gamma, \tag{3.1}$$

which is called the *eqicentroaffine curvature*. Introducing the frame $\Psi(x) = [\Gamma, \Gamma_x] \in \mathrm{SL}(2)$, we have

$$\Psi_x = \Psi U, \quad U = \begin{bmatrix} 0 & -u \\ 1 & 0 \end{bmatrix}, \tag{3.2}$$

which is called the Frenet formula of the equicentroaffine plane curves. Now we introduce a continuous deformation parameter $t \in \mathbb{R}$, and consider a deformation of $\Gamma = \Gamma(x,t)$ given by

$$\Gamma_t = 2u\Gamma_x - u_x\Gamma. \tag{3.3}$$

Then (3.3) is rewritten in terms of $\Psi = \Psi(x,t)$ as

$$\Psi_t = \Psi V, \quad V = \begin{bmatrix} u_x & 2u \\ -2u^2 - u_{xx} & -u_x \end{bmatrix}. \tag{3.4}$$

Then this deformation preserves the area $\det[\Gamma, \Gamma_x]$, namely $\frac{\partial}{\partial t}\det[\Gamma, \Gamma_x] = 0$, and the compatibility condition $\Psi_{xt} = \Psi_{tx}$ of the system of partial differential equations (3.2) and (3.4) yields the KdV equation

$$u_t = u_{xxx} + 6uu_x. \tag{3.5}$$

We call the motion of equicentroaffine plane curves (3.3) the KdV flow on the smooth equicentroaffine plane curves.

## 3.2 Semi-discrete KdV flow on discrete equicenroaffine plane curves

In this section, we review the semi-discrete KdV flow on discrete equicentoraffine plane curves [5].

Let $\Gamma_n : \mathbb{Z} \to \mathbb{R}^2$ be a discrete plane curve in the equicentroaffine geometry. If $\Gamma_n$ satisfies $a_n := \det[\Gamma_n, \Gamma_{n+1}] \neq 0$ for all $n$, then we call $\Gamma_n$ the discrete equicentroaffine plane curve. Also, assuming

$$a_n + a_{n-1} = \det[\Gamma_n, \Gamma_{n+1} - \Gamma_{n-1}] \neq 0, \tag{3.6}$$

which means that the end point of $\Gamma_{n+1}$ is not on the line $\Gamma_{n-1} + \mathbb{R}\Gamma_n$, we have

$$0 = \det\left[\Gamma_n, \frac{\Gamma_{n+1} - \Gamma_n}{a_n}\right] - \det\left[\Gamma_n, \frac{\Gamma_n - \Gamma_{n-1}}{a_{n-1}}\right] \tag{3.7}$$

$$= \det\left[\Gamma_n, \frac{\Gamma_{n+1} - \Gamma_n}{a_n} - \frac{\Gamma_n - \Gamma_{n-1}}{a_{n-1}}\right]. \tag{3.8}$$

Then there exists a function $\kappa_n : \mathbb{Z} \to \mathbb{R}$ such that

$$\frac{1}{a_n + a_{n-1}} \left( \frac{\Gamma_{n+1} - \Gamma_n}{a_n} - \frac{\Gamma_n - \Gamma_{n-1}}{a_{n-1}} \right) = -\kappa_n \Gamma_n. \tag{3.9}$$

In terms of the frame $\Psi_n = \left[ \Gamma_n, \frac{\Gamma_{n+1} - \Gamma_n}{a_n} \right] \in \mathrm{SL}(2)$, (3.9) is rewritten as

$$\Psi_{n+1} = \Psi_n U_n, \quad U_n = \begin{bmatrix} 1 & -(a_{n+1} + a_n)\kappa_{n+1} \\ a_n & 1 - a_n(a_{n+1} + a_n)\kappa_{n+1} \end{bmatrix}, \tag{3.10}$$

which is called the Frenet formula of discrete equicentroaffine plane curves. Now we assume that $a_n = a$ is a constant and define the function $u_n$ by

$$u_n = 1 - a^2 \kappa_n, \tag{3.11}$$

Then (3.10) is rewritten as

$$\Psi_{n+1} = \Psi_n U_n, \quad U_n = \begin{bmatrix} 1 & 2(u_{n+1} - 1)/a \\ a & 2u_{n+1} - 1 \end{bmatrix}. \tag{3.12}$$

Now we introduce continuous deformation parameter $t \in \mathbb{R}$, and consider a deformation of $\Gamma_n = \Gamma_n(t)$ given by

$$\frac{d}{dt}\Gamma_n = \frac{1}{a} \left( \frac{1}{u_n} \Gamma_{n+1} - \Gamma_n \right). \tag{3.13}$$

This deformation is rewritten, in terms of the frame $\Psi_n = \Psi_n(t)$, as

$$\frac{d}{dt}\Psi_n = \Psi_n V_n, \quad V_n = \frac{1}{a} \begin{bmatrix} \frac{1}{u_n} - 1 & \frac{1}{a}\left(2 - \frac{1}{u_n} - \frac{1}{u_{n+1}}\right) \\ \frac{a}{u_n} & 1 - \frac{1}{u_n} \end{bmatrix}. \tag{3.14}$$

Then the deformation preserves the area $\det[\Gamma_n, \Gamma_{n+1}]$, namely $\frac{d}{dt}\det[\Gamma_n, \Gamma_{n+1}] = 0$, and the compatibility condition of the partial difference and differential equations (3.12) and (3.14) yields the semi-discrete KdV equation:

$$\frac{d}{dt}u_n = \frac{1}{2a} \left( \frac{1}{u_{n+1}} - \frac{1}{u_{n-1}} \right). \tag{3.15}$$

We call the motion of discrete equicentroaffine plane curves (3.13) the semi-discrete KdV flow on the discrete equicentroaffine plane curves.

# 4 Miura transformation

It is well-known that there is a transformation between solutions to the (defocusing) mKdV equation and the KdV equation, which is called the *Miura transformation* [42]. Accordingly it is expected that there is a close relationship between curve flows in centroaffine geometry and equicentroaffine geometry. In this chapter, we establish concrete correspondences between curve flows on centroaffine plane curves and equicentroaffine plane curves for both smooth and semi-discrete cases.

## 4.1 Correspondence between motions of smooth plane curves

In this section, we present a relationship between the defocusing mKdV flow on centroaffine plane curves and the KdV flow on equicentroaffine plane curves by using the Miura transformation. We start with the introduction to a part of the Miura transformation.

**Proposition 4.1 (Miura transformation [42])** *If $\kappa = \kappa(x,t)$ satisfies the defocusing mKdV equation (2.16), then a function $\overline{u}$ defined by*

$$\overline{u} = \frac{\kappa_x}{2} j - \frac{\kappa^2}{4}, \tag{4.1}$$

*where $j$ is a split complex number, namely $j^2 = 1$, satisfies the KdV equation (3.5).*

For a centroaffine plane curve $\gamma = \gamma(x,t)$, where $x$ is the centroaffine arclength parameter at each time $t$, we can assume $\det[\gamma, \gamma_x] > 0$ by a parameter change $x \mapsto -x$ if necessary. For a solution $\gamma$ to the defocusing mKdV flow (2.14), we define a new curve flow $\overline{\Gamma} = \overline{\Gamma}(x,t)$ by

$$\overline{\Gamma} = h\gamma, \quad h = (\det[\gamma, \gamma_x])^{-1/2}. \tag{4.2}$$

Then we immediately have from (4.2)

$$\det\left[\overline{\Gamma}, \overline{\Gamma}_x\right] = h^2 \det[\gamma, \gamma_x] = 1. \tag{4.3}$$

Moreover, differentiating $h$ with respect to $x$ and $t$, we get

$$\begin{aligned} h_x &= -\frac{1}{2}(\det[\gamma, \gamma_x])^{-3/2} \det[\gamma, \gamma_{xx}] \\ &= -\frac{\kappa}{2}(\det[\gamma, \gamma_x])^{-1/2}, \end{aligned}$$

and

$$
\begin{aligned}
h_t &= -\frac{1}{2}\left(\det\left[\gamma,\gamma_x\right]\right)^{-3/2}\left(\det\left[\gamma_t,\gamma_x\right]+\det\left[\gamma,\gamma_{xt}\right]\right)\\
&= \left(\frac{\kappa^3}{4}-\frac{\kappa_{xx}}{2}\right)\left(\det\left[\gamma,\gamma_x\right]\right)^{-1/2},
\end{aligned}
$$

which yield

$$
\frac{h_x}{h} = -\frac{\kappa}{2}, \tag{4.4}
$$

$$
\frac{h_t}{h} = -\frac{\kappa_{xx}}{2}+\frac{\kappa^3}{4}, \tag{4.5}
$$

respectively. Here we have used (2.5) and (2.14). Now we put a function $\overline{u} = \overline{u}(x,t)$ as

$$
\overline{u} = \frac{\kappa_x}{2}-\frac{\kappa^2}{4}. \tag{4.6}
$$

Then differentiating $\overline{\Gamma}$ with respect to $x$, we have from (4.4) and (2.5)

$$
\overline{\Gamma}_x = h_x\gamma+h\gamma_x = h\left(-\frac{\kappa}{2}\gamma+\gamma_x\right), \tag{4.7}
$$

and

$$
\begin{aligned}
\overline{\Gamma}_{xx} &= h_x\left(-\frac{\kappa}{2}\gamma+\gamma_x\right)+h\left(-\frac{\kappa_x}{2}\gamma-\frac{\kappa}{2}\gamma_x+\gamma_{xx}\right)\\
&= h\left(\frac{\kappa^2}{4}-\frac{\kappa_x}{2}-\lambda\right)\gamma\\
&= -\left(\overline{u}+\lambda\right)\overline{\Gamma}.
\end{aligned} \tag{4.8}
$$

On the other hand, differentiating $\overline{\Gamma}$ with respect to $t$ we get from (2.14), (4.5) and (4.7)

$$
\begin{aligned}
\overline{\Gamma}_t &= h_t\gamma+h\gamma_t\\
&= h\left(\frac{\kappa^3}{4}-\frac{\kappa_{xx}}{2}+2\lambda\kappa\right)\gamma+h\left(\kappa_x-\frac{\kappa^2}{2}-4\lambda\right)\gamma_x\\
&= \left(\frac{\kappa\kappa_x}{2}-\frac{\kappa_{xx}}{2}\right)\overline{\Gamma}+\left(\kappa_x-\frac{\kappa^2}{2}-4\lambda\right)\overline{\Gamma}_x\\
&= -\overline{u}_x\overline{\Gamma}+2\left(\overline{u}-2\lambda\right)\overline{\Gamma}_x.
\end{aligned} \tag{4.9}
$$

Therefore the frame given by $\overline{\Psi} = [\overline{\Gamma}, \overline{\Gamma}_x]$, satisfies the system of differential equations $\overline{\Psi}_x = \overline{\Psi}\overline{U}$ and $\overline{\Psi}_t = \overline{\Psi}\overline{V}$, where

$$\overline{U} = \begin{bmatrix} 0 & -\overline{u} - \lambda \\ 1 & 0 \end{bmatrix},$$
$$\overline{V} = \begin{bmatrix} -\overline{u}_x & -2(\overline{u} + \lambda)(\overline{u} - 2\lambda) - \overline{u}_{xx} \\ 2(\overline{u} - 2\lambda) & \overline{u}_x \end{bmatrix},$$

which gives a Lax pair for the KdV equation $\overline{u}_t = \overline{u}_{xxx} + 6\overline{u}\,\overline{u}_x$, with a spectral parameter $\lambda$. Introducing the Galilean transformation

$$s = x - 6\lambda t, \tag{4.10}$$

we see that the curve $\Gamma(s,t) = \overline{\Gamma}(x,t)$ satisfies (3.1) and (3.3) with $u(s,t) = \overline{u}(x,t) + \lambda$. Thus, (4.2) with (4.10) is the Miura transformation between the defocusing mKdV flow (2.14) on centroaffine plane curves and the KdV flow (3.3) on equicentroaffne plane curves.

## 4.2 Correspondence between motions of discrete plane curves

In this section, we present a relationship between the Lotka-Volterra flow on discrete centroaffine plane curves and the semi-discrete KdV flow on discrete equicentroaffine plane curves.

Let $\gamma_n = \gamma_n(t)$ be the Lotka-Volterra flow on a discrete centroaffine plane curve, described in Section 2.2. We define a new discrete curve flow $\overline{\Gamma}_n = \overline{\Gamma}_n(t)$ and a function $\overline{u}_n = \overline{u}_n(t)$ by

$$\overline{\Gamma}_n = h_n(t)\gamma_n, \quad \overline{u}_{n+1}\overline{u}_n = -\frac{1}{4\varepsilon v_n}, \tag{4.11}$$

where $h_n = h_n(t)$ is determined by

$$h_{n+1}h_n \det[\gamma_n, T_n] = 1. \tag{4.12}$$

Then we immediately have from (4.11)

$$\det[\overline{\Gamma}_n, \overline{\Gamma}_{n+1}] = \varepsilon.$$

Then switching the parameter $n$ of the equation (4.12), we get

$$h_{n+2}h_{n+1} \det[\gamma_{n+1}, T_{n+1}] = h_{n+1}h_n \det[\gamma_n, T_n], \tag{4.13}$$

which yields from (2.39)

$$v_n = -\frac{1}{\varepsilon}\frac{h_n}{h_{n+2}}. \tag{4.14}$$

On the other hand, differentiating (4.12) with respect to $t$, we have from (2.39)

$$\begin{aligned} 0 &= \frac{d}{dt}(h_{n+1}h_n)\det[\gamma_n, T_n] + h_{n+1}h_n\left(\det\left[\frac{dT_n}{dt}, \gamma_n\right] + \det\left[T_n, \frac{d\gamma_n}{dt}\right]\right) \\ &= \left(\frac{dh_{n+1}}{dt}h_n + h_{n+1}\frac{dh_n}{dt} - 2h_{n+1}h_n(v_n + v_{n-1})\right)\det[\gamma_n, T_n], \end{aligned} \tag{4.15}$$

which is rewritten as

$$\frac{1}{h_{n+1}}\frac{dh_{n+1}}{dt} + \frac{1}{h_n}\frac{dh_n}{dt} = 2h_{n+1}h_n(v_n + v_{n-1}), \tag{4.16}$$

and it implies

$$\frac{1}{h_n}\frac{dh_n}{dt} = 2v_{n-1}. \tag{4.17}$$

Then substituting (4.14) into (4.17), we get

$$\frac{1}{h_n}\frac{dh_n}{dt} = -\frac{2}{\varepsilon}\frac{h_{n-1}}{h_{n+1}}. \tag{4.18}$$

Now we consider the Frenet equation and the deformation equation of $\overline{\Gamma}_n$. Noticing that

$$\Phi_{n-1} = -\frac{1}{\varepsilon v_{n-1}}\Phi_n\begin{bmatrix} 0 & -v_{n-1} \\ -\varepsilon & 1 \end{bmatrix}, \tag{4.19}$$

we have

$$\begin{aligned} \overline{\Gamma}_{n+1} - 2\overline{\Gamma}_n + \overline{\Gamma}_{n-1} &= h_{n+1}\gamma_{n+1} - 2h_n\gamma_n + h_{n-1}\gamma_{n-1} \\ &= (h_{n+1} - 2h_n)\gamma_n + \left(\varepsilon h_{n+1} + \frac{h_{n-1}}{v_{n-1}}\right)T_n. \end{aligned} \tag{4.20}$$

We can easily verify that the coefficient of $T_n$ of (4.20) vanishes by (4.14). Therefore we obtain

$$\overline{\Gamma}_{n+1} - 2\overline{\Gamma}_n + \overline{\Gamma}_{n-1} = \left(\frac{h_{n+1}}{h_n} - 2\right)\overline{\Gamma}_n. \tag{4.21}$$

Now we consider the deformation equation of $\overline{\Gamma}_n$. Differentiating $\overline{\Gamma}_n$ with respect to $t$, we have

$$\begin{aligned} \frac{d}{dt}\overline{\Gamma}_n &= \frac{dh_n}{dt}\gamma_n + h_n\frac{d\gamma_n}{ds} \\ &= \left(\frac{1}{h_n}\frac{dh_n}{dt} - 2v_{n-1} - \frac{1}{\varepsilon}\right)\overline{\Gamma}_n + \frac{2}{\varepsilon}\frac{h_n}{h_{n+1}}\overline{\Gamma}_{n+1}, \end{aligned} \tag{4.22}$$

which yields from (4.18)

$$\frac{d}{dt}\overline{\Gamma}_n = \frac{1}{\varepsilon}\left(\frac{2h_n}{h_{n+1}}\overline{\Gamma}_{n+1} - \overline{\Gamma}_n\right). \tag{4.23}$$

On the other hand, we obtain by substituting (4.14) into (4.11)

$$\frac{h_{n+1}}{h_n} = 2\overline{u}_n. \tag{4.24}$$

Finally, the Frenet equation (4.21) and the deformation equation (4.23) of $\overline{\Gamma}_n$ are rewritten from (4.24) as

$$\overline{\Gamma}_{n+1} - 2\overline{\Gamma}_n + \overline{\Gamma}_{n-1} = -2(1-\overline{u}_n)\overline{\Gamma}_n, \tag{4.25}$$

$$\frac{d}{dt}\overline{\Gamma}_n = \frac{1}{\varepsilon}\left(\frac{1}{\overline{u}_n}\overline{\Gamma}_{n+1} - \overline{\Gamma}_n\right), \tag{4.26}$$

respectively. Then we see that the curve $\Gamma_n(t) = \overline{\Gamma}_n(t)$ satisfies (3.9) and (3.13) with $u_n(t) = \overline{u}_n(t)$. Namely, $\overline{\Gamma}_n(t)$ is the semi-discrete KdV flow on equicentroaffine plane curves. Therefore, (4.11) with (4.12) is the Miura transformation between the Lotka-Volterra flow on centroaffine plane curves and the semi-discrete KdV flow on equicentroaffine plane curves.

# 5 Integrable deformations of discrete space curves and its application to linkage mechanisms

We consider a particular class of linkage mechanisms, which can be described the semi-discrete mKdV and the semi-discrete sine-Gordon flows on discrete space curves. In this Chapter, a mathematical analysis of linkages is discussed based on the paper [11].

A linkage is a mechanical system consisting of rigid bodies (called links) joined together by joints. Mathematical study of linkage dates back to Euler, Chebyshev, Sylvester, Kempe, and Cayley and since then the topology and the geometry of the configuration space have attracted many researchers (see [36,48,55] for a survey). Most of the research focuses on *pin joint linkages*, which consist of only one type of joint called pin joints. A pin joint constrains the positions of ends of adjacent links to stay together. To a pin joint linkage we can associate a graph whose vertices are joints and edges are links, where edges are assigned its length. The state of a pin joint linkage is effectively specified by the coordinates of the joint positions, where the distance of two joints connected by a link is constrained

to its length. Thus, its configuration space can be modelled by the space of isometric imbeddings of the corresponding graph to some Euclidean space. Note that in practice, joints and links have sizes and they collide to have limited mobility, but here we consider ideal linkages with which joints and links can pass through each other.

While the configuration spaces of (especially planar) pin joint linkages are well studied, there are other types of linkages which are not so popular. In this thesis, we are mainly interested in linkages consisting of hinges (revolute joints). To set up a framework to study linkages with various types of joints, we first introduce a mathematical model of general linkages as graphs decorated with groups (Section 5.1), extending previous approaches (see [58] and references therein). This formulation can be viewed as a special type of constraint network (e.g., [38]). Then in Section 5.2, we focus on linkages consisting of hinges. Unlike a pin joint which constrains only the relative positions of connected links, a hinge has an axis so that it also constrains the relative orientation of connected links.

We are particularly interested in a simple case when $n$ links in $\mathbb{R}^3$ are joined by hinges to form a circle (Section 5.3). Such a linkage can be roughly thought of as a discrete closed space curve, where hinge axes are identified with the lines spanned by the binormal vectors. Properties of such linkages can thus be translated and stated in the language of discrete curves. An example of such linkage is the threefold symmetric Bricard 6R linkage consisting of six hinges (Figure 2), which exhibits a turning-over motion and has the configuration space homeomorphic to a circle. As a generalization to the threefold symmetric Bricard 6R linkage, we consider a family of linkages consisting of copies of an identical links connected by hinges, which we call Kaleidocycles, and they are characterized as discrete curves of constant speed and constant torsion.

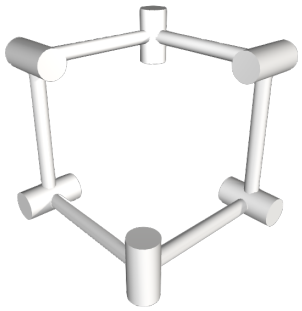

Figure 2: Threefold symmetric Bricard 6R linkage.

The motion of Kaleidocycles corresponds to isoperimetric and torsion-preserving deformation of discrete closed space curves of constant torsion. In Section 5.4,

we define a flow on the configuration space of a Kaleidocycle by the semi-discrete mKdV and the semi-discrete sine-Gordon equations. This flow generates the characteristic turning-over motion of the Kaleidocycle.

Kaleidocycles exhibit interesting properties and pose some topological and geometrical questions. In Section 5.6 we indicate some directions of further study to close this exposition.

Mobility analysis of a linkage mechanism studies how many degrees of freedom a particular state of the linkage has, which corresponds to determination of the local dimension at a point in the configuration space (see, for example, [59]). On the other hand, rigidity of linkages consisting of hinges are studied in the context of the body-hinge framework (see, for example, [44, 49]). The main focus of the study is to give a characterization for a generic linkage to have no mobility. That is, the question is to see if the configuration space is homeomorphic to a point or isolated points.

Sato and Tanaka [66] study the motion of a certain linkage mechanism with a constrained degree of freedom and observed that soliton solutions appear.

Closed (continuous) curves of constant torsion have attracted sporadic interest of geometers, e.g., [25, 29, 43, 69, 70]. In particular, [30] discusses an evolution of a constant torsion curve governed by a sine-Gordon equation in the continuous setting.

## 5.1 A mathematical model of linkage

In this section, we set up a general mathematical model of linkages. We define an abstract linkage as a decorated graph, and its realization as a certain imbedding of the graph in a Euclidean space. Our definition generalizes the usual graphical model of a pin joint linkage to allow different types of joints.

Denote by $SO(n)$ the group of orientation preserving linear isometries of the $n$-dimensional Euclidean space $\mathbb{R}^n$. An element of $SO(n)$ is identified with a sequence of $n$-dimensional column vectors $[f_1, f_2, \dots, f_n]$ which are mutually orthogonal and have unit length with respect to the standard inner product $\langle x, y\rangle$ of $x, y \in \mathbb{R}^n$. Denote by $SE(n)$ the group of $n$-dimensional orientation preserving Euclidean transformations. That is, it consists of the affine transformations $\mathbb{R}^n \to \mathbb{R}^n$ which preserves the orientation and the standard metric. We represent the elements of $SE(n)$ by $(n+1)\times(n+1)-$homogeneous matrices acting on

$$\mathbb{R}^n \simeq \{{}^t(x_1, x_2, \dots, x_n, 1) \in \mathbb{R}^{n+1}\}$$

by multiplication from the left. For example, an element of $SE(3)$ is represented

by a matrix

$$\begin{pmatrix} a_{11} & a_{12} & a_{13} & l_1 \\ a_{21} & a_{22} & a_{23} & l_2 \\ a_{31} & a_{32} & a_{33} & l_3 \\ 0 & 0 & 0 & 1 \end{pmatrix}.$$

The vector $l = {}^t(l_1, l_2, l_3)$ is called the translation part. The upper-left $3 \times 3$-block of $A$ is called the linear part and denoted by $\bar{A} \in SO(3)$. Thus, the action on $v \in \mathbb{R}^3$ is also written by $v \mapsto \bar{A}v + l$.

**Definition 5.1** *An n-dimensional* abstract linkage *L consists of the following data:*

- *a connected oriented finite graph* $G = (V, E)$
- *a subgroup* $J_v \subset SE(n)$ *assigned to each* $v \in V$*, which defines the joint symmetry*
- *an element* $C_e \in SE(n)$ *assigned to each* $e \in E$*, which defines the link constraint.*

In practical applications, we are interested in the case when $n = 2$ or 3. When $n = 2$ linkages are said to be *planar*, and when $n = 3$ linkages are said to be *spatial*.

We say a linkage $L$ is *homogeneous* if for any pair $v_1, v_2 \in V$, the following conditions are satisfied:

- there exists a graph automorphism which maps $v_1$ to $v_2$ (i.e., $Aut(G)$ acts transitively on $V$),
- $J_{v_1} = J_{v_2}$,
- and $C_{e_1} = C_{e_2}$ for any $e_1, e_2 \in E$.

A *state* or *realization* $\phi$ of an abstract linkage $L$ is an assignment of a coset to each vertex

$$\phi : v \mapsto SE(n)/J_v$$

such that for each edge $e = (v_1, v_2) \in E$, the following condition is satisfied:

$$\phi(v_2)J_{v_2} \cap \phi(v_1)J_{v_1}C_e \neq \emptyset, \tag{5.1}$$

where cosets are identified with subsets of $SE(n)$.

Let us give an intuitive description of (5.1). Imagine a reference joint sitting at the origin in a reference orientation. The subset $\phi(v_1)J_{v_1}$ consists of all the rigid

transformations which maps the reference joint to the joint at $v_1$ with a specified position and an orientation $\phi(v_1)$ up to the joint symmetry $J_{v_1}$. The two subsets $\phi(v_2)J_{v_2}$ and $\phi(v_1)J_{v_1}C_e$ intersects if and only if the joint at $v_1$ can be aligned to that at $v_2$ by the transformation $C_e$.

**Example 5.2** *The usual pin joints $v_1, v_2$ connected by a bar-shaped link $e$ of length $l$ are represented by $J_{v_1} = J_{v_2} = SO(n)$ and $C_e$ being any translation by $l$. Note that $SE(3)/J_{v_1} \simeq \mathbb{R}^3$. It is easy to see that (5.1) amounts to saying the difference in the translation part of $\phi(v_2)$ and $\phi(v_1)$ should have the norm equal to $l$.*

*Two revolute joints (hinges) $v_1, v_2$ in $\mathbb{R}^3$ connected by a link $e$ of length $l$ making an angle $\alpha$ are represented by $J_{v_1} = J_{v_2}$ being the group generated by rotations around the $z$-axis and the $\pi$-rotation around the $x$-axis, and $C_e$ being the rotation by $\alpha$ around $x$-axis followed by the translation along $x$-axis by $l$; that is*

$$J_{v_1} = J_{v_2} = \left\{ \begin{pmatrix} \cos\theta & \mp\sin\theta & 0 & 0 \\ \sin\theta & \pm\cos\theta & 0 & 0 \\ 0 & 0 & \pm 1 & 0 \\ 0 & 0 & 0 & 1 \end{pmatrix} \middle| \, \theta \in \mathbb{R} \right\}, C_e = \begin{pmatrix} 1 & 0 & 0 & l \\ 0 & \cos\alpha & -\sin\alpha & 0 \\ 0 & \sin\alpha & \cos\alpha & 0 \\ 0 & 0 & 0 & 1 \end{pmatrix}.$$

*Note that $SE(3)/J_{v_1}$ is the space of based lines (i.e., lines with specified origins) in $\mathbb{R}^3$, and the line is identified with the axis of the hinge.*

The space $\overline{\mathscr{C}}(L)$ of all realizations of a given linkage $L$ admits an action of $SE(n)$ defined by $\phi \mapsto g\phi(v)$ for $g \in SE(n)$. The quotient of $\overline{\mathscr{C}}(L)$ by $SE(n)$ is denoted by $\mathscr{C}(L)$ and called the *configuration space* of $L$. Each connected component of $\mathscr{C}(L)$ corresponds to the mobility of the linkage $L$ in a certain state. When a connected component is a manifold, its dimension is what mechanists call *the (internal) degrees of freedom* (DOF, for short). Given a pair of points on $\mathscr{C}(L)$, the problem of finding an explicit path connecting the points is called *motion planning* and has been one of the main topics in mechanics [54]. In a similar manner, many questions about a linkage can be phrased in terms of the topology and the geometry of its configuration space.

**Example 5.3** *Consider the following spatial linkages consisting of pin joints depicted in Figure 3. In the latter, we assume the two joints $a$ and $b$ are fixed to the wall. Up to the action of the global rigid transformation $SE(3)$, these two linkages are equivalent and share the same configuration space $\mathscr{C}(L)$; in the left linkage, the global action is killed by fixing the positions of three joints except for $p$. The topology of $\mathscr{C}(L)$ changes with respect to the parameter $l$ which is the length of*

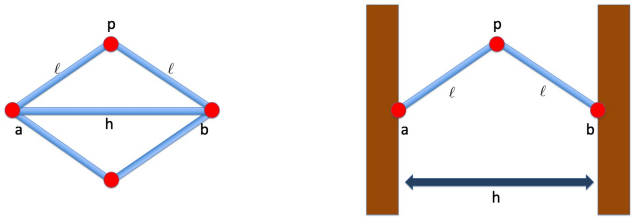


Figure 3: Example of equivalent pin joint linkages.

*the bars. Namely, we have*

$$\mathscr{C}(L) = \{x_p \in \mathbb{R}^3 \mid |x_p - x_a|^2 = |x_p - x_b|^2 = l^2\} = \begin{cases} S^1 & (l > 2h) \\ pt & (l = 2h) \\ \emptyset & (l < 2h) \end{cases}.$$

*This seemingly trivial example is indeed related to a deeper and subtle question on the topology of the configuration space; the space is identified with the* real *solutions to a system of algebraic equations.*

## 5.2 Hinged linkage in three space

Now, we focus on a class of spatial linkages consisting of hinges, known also as three dimensional body-hinge frameworks [44]. In this case, the definition in the previous section can be reduced to a simpler form.

Notice that in $\mathbb{R}^3$ a pair of hinges connected by a link can be modelled by a tetrahedron. A hinge is an isometrically embedded real line in $\mathbb{R}^3$. Given a pair of hinges, unit-length segments on the hinges containing the base points in the centre span a tetrahedron, or a quadrilateral when the two hinges are parallel (see Figure 4 Left). It is sometimes convenient to decompose the link constraint $C_{(v_1,v_2)} \in SE(3)$ into three parts; a translation along the hinge direction at $v_1$, a screw motion along an axis perpendicular to both hinges, and a translation along the hinge direction at $v_2$. This corresponds to a common presentation among mechanists called the Denavit–Hartenberg parameters [33]. We can find the decomposition geometrically as follows: Find a line segment which is perpendicular to the both hinges connected by the link $e$, which we call the *core segment*. It is unique unless the hinges are parallel. The intersection points of the core segment and the hinges are called the *marked* points. Form a tetrahedron from the line segments on hinges containing the marked points in the centre. By construction, this tetrahedron has a special shape that the line connecting the centre of two hinge edges (the core segment) is perpendicular to the hinge edges. Such a tetrahedron

is called a *disphenoid*. The shape of the disphenoid defines a screw motion along the core segment up to a $\pi$-rotation. The translations along the hinge directions are to match the marked points to the base points (see Figure 4). To sum up, a spatial hinged linkage can be considered as a collection of lines connected by disphenoids at marked points. Thus, we arrive in the following definition.

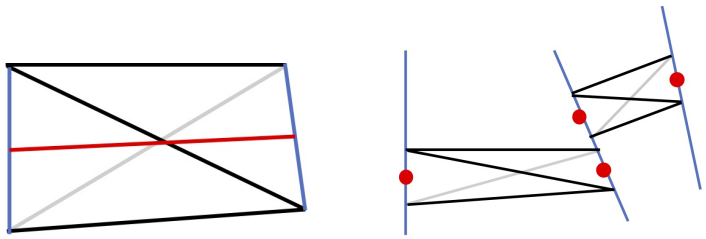

Figure 4: Left: a disphenoid formed by two hinge edges, Right: three hinges connected by disphenoids. The dots indicate the marked points.

**Definition 5.4** *A* hinged network *consists of*

- *a connected oriented finite graph* $G = (V, E)$,
- *two edge labels* $\nu : E \to [0, \pi)$ *called the* torsion angle *and* $\varepsilon : E \to \mathbb{R}_{\geq 0}$ *called the* segment length,
- *and a vertex label* $\iota_v : E(v) \to \mathbb{R}$ *called the* marking, *where* $E(v) \subset E$ *is the set of edges adjacent to* $v \in V$.

*A state of a hinged network is an assignment to each vertex* $v \in V$ *of an isometric embedding* $h_v : \mathbb{R} \to \mathbb{R}^3$ *such that for any* $(v_1, v_2) \in E$

1. $|l| = \varepsilon(v_1, v_2)$, *where* $l = h_{v_1} \circ \iota_{v_1}(v_1, v_2) - h_{v_2} \circ \iota_{v_2}(v_1, v_2)$
2. $l \perp h_{v_1}(\mathbb{R})$ *and* $l \perp h_{v_2}(\mathbb{R})$
3. $\angle h_{v_1}(\mathbb{R}) h_{v_2}(\mathbb{R}) = \nu$, *where the angle is measured in the left-hand screw manner with respect to* $l$.

*Intuitively,* $h_v(\mathbb{R})$ *is the line spanned by the hinges, and the first two conditions demand that the marked points are connected by the core segments* $l$, *whereas the last condition dictates the torsion angle of adjacent hinges* $h_{v_1}(\mathbb{R})$ *and* $h_{v_2}(\mathbb{R})$.

A hinged network is said to be *serial* when the graph $G$ is a line graph; i.e., a connected graph of the shape $\bullet \to \bullet \to \bullet \to \cdots \to \bullet$. It is said to be *closed* when the graph $G$ is a circle graph; i.e., a connected finite graph with every vertex having outgoing degree one and incoming degree one. A hinged network is homogeneous if

- $Aut(G)$ acts on $G$ transitively,
- $\nu(e), \varepsilon(e)$, and $\iota_v$ do not depend on $e \in E$ and $v \in V$. That is, it is made of congruent tetrahedral links.

**Example 5.5** *A planar pin joint linkage is a special type of hinged network with $\nu(e) = 0$ for all $e \in E$ and $\iota_v = 0$ for all $v \in V$. That is, all hinges are parallel and marked points are all at the origin. On the other hand, any hinged network can be thought of as a spatial pin joint linkage by replacing every tetrahedral link with four bar links connected by four pin joints forming the tetrahedron. Therefore, hinged networks form an intermediate class of linkages which sits between planar pin joint linkages and spatial pin joint linkages.*

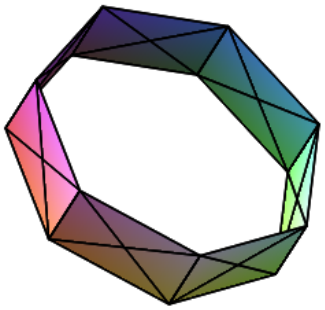

Figure 5: A degenerate hinged network over a circle corresponding to a planar six-bar pin joint linkage.

**Example 5.6** *The hinged network depicted in Figure 6 is over the wedge sum of two circle graphs. It exhibits a jump roping motion. A similar but more complex network is found in [31, Section 6].*

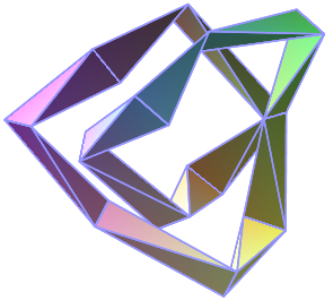

Figure 6: A hinged network over the wedge of two circles.

**Example 5.7** *Closed hinged networks with $\varepsilon(e) = 0$ (that is, adjacent hinge lines intersect) for all $e \in E$ provide a linkage model for discrete* developable strips *studied recently by K. Naokawa and C. Müller (see Figure 7). They are made of (planar) quadrilaterals joined together by the pair of non-adjacent edges as hinges.*

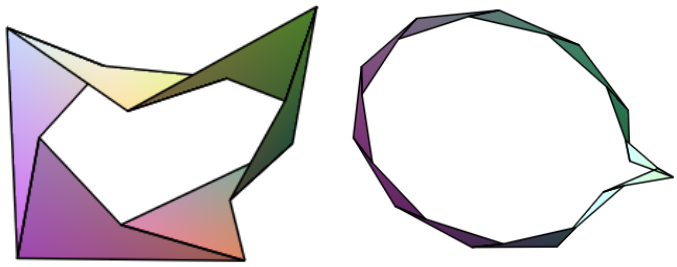

Figure 7: Developable discrete Möbius strip consisting of 6 (respectively 12) congruent quadrilateral links.

## 5.3 Hinged network and discrete space curve

In this section, we describe a connection between spatial closed hinged networks and discrete closed space curves. This connection is the key idea of this chapter which provides a way to study certain linkages using tools in discrete differential geometry.

First, we briefly review the basic formulation of discrete space curves (see, for example, [1]). A *discrete space curve* is a map

$$\gamma : \mathbb{Z} \to \mathbb{R}^3, \quad (i \mapsto \gamma_n).$$

For simplicity, in this chapter we always assume that $\gamma_n \neq \gamma_{n+1}$ for any $n$ and that three points $\gamma_{-1}$, $\gamma_0$ and $\gamma_1$ are not colinear. The *tangent vector* $T : \mathbb{Z} \to S^2$ is defined by

$$T_n = \frac{\gamma_{n+1} - \gamma_n}{\varepsilon_n}, \quad \varepsilon_n = |\gamma_{n+1} - \gamma_n|. \tag{5.2}$$

We say $\gamma$ has a constant speed of $\varepsilon$ if $\varepsilon_n = \varepsilon$ for all $n$. A discrete space curve with a constant speed is sometimes referred to as an *arc length parametrized curve* [41].

The *normal vector* $N : \mathbb{Z} \to S^2$ and the *binormal vector* $B : \mathbb{Z} \to S^2$ are defined by

$$B_n = \begin{cases} \frac{T_{n-1} \times T_n}{|T_{n-1} \times T_n|} & (T_{n-1} \times T_n \neq 0) \\ B_{n-1} & (T_{n-1} \times T_n = 0 \text{ and } n > 0) \\ B_{n+1} & (T_{n-1} \times T_n = 0 \text{ and } n < 0), \end{cases} \tag{5.3}$$

$$N_n = B_n \times T_n, \tag{5.4}$$

respectively. Then, $[T_n, N_n, B_n] \in SO(3)$ is called the *Frenet frame* of $\gamma$. For our purpose, it is more convenient to use a modified version of the ordinary Frenet frame, which we define as follows. Set $b_0 = B_0$ and define $b_n = \pm B_n$ recursively so that $\langle b_n \times b_{n-1}, T_{n-1} \rangle \geq 0$ and $\langle b_{n-1}, b_n \rangle \neq -1$. Then, $\Phi_n = [T_n, \widetilde{N}_n, b_n] \in SO(3)$, where $\widetilde{N}_n = b_n \times T_n$ (see Figure 8).

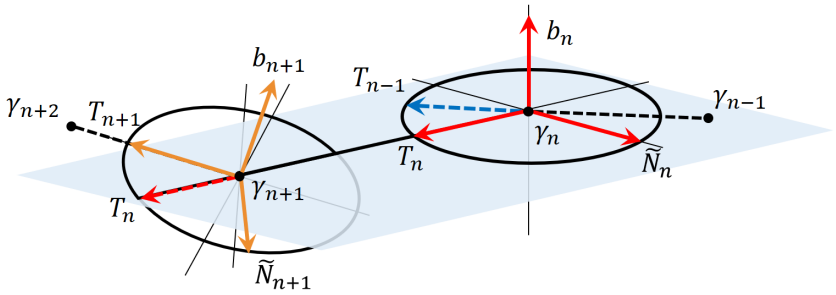


Figure 8: A discrete space curve with the frame $\Phi_n$.

For $\theta \in \mathbb{R}$, we define $R_1(\theta), R_3(\theta) \in SO(3)$ by

$$R_1(\theta) = \begin{bmatrix} 1 & 0 & 0 \\ 0 & \cos\theta & -\sin\theta \\ 0 & \sin\theta & \cos\theta \end{bmatrix}, \quad R_3(x) = \begin{bmatrix} \cos\theta & -\sin\theta & 0 \\ \sin\theta & \cos\theta & 0 \\ 0 & 0 & 1 \end{bmatrix}. \tag{5.5}$$

There exist $\kappa : \mathbb{Z} \to [-\pi, \pi)$ and $\nu : \mathbb{Z} \to [0, \pi)$ such that

$$\Phi_{n+1} = \Phi_n L_n, \quad L_n = R_1(-\nu_{n+1}) R_3(\kappa_{n+1}). \tag{5.6}$$

We call $\kappa$ the *signed curvature angle* and $\nu$ the *torsion angle*. Figure 9 illustrates how to obtain $\Phi_{n-1}$ from $\Phi_n$ by (5.6). Note that we have

$$\begin{gathered} \langle T_n, T_{n-1} \rangle = \cos\kappa_n, \quad \langle b_n, b_{n-1} \rangle = \cos\nu_n, \quad \langle b_n, \widetilde{N}_{n-1} \rangle = \sin\nu_n, \\ \langle b_n, T_n \rangle = \langle b_{n+1}, T_n \rangle = 0. \end{gathered} \tag{5.7}$$

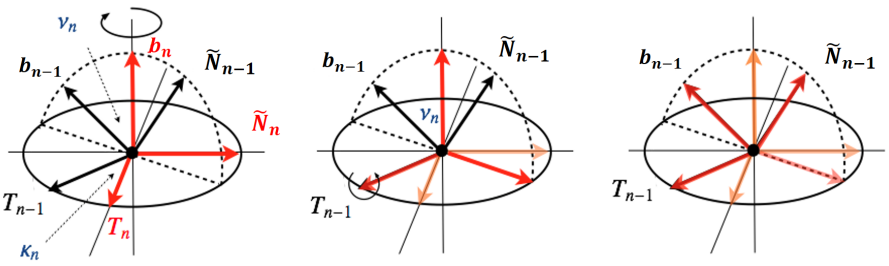


Figure 9: The curvature angle $\kappa$ and the torsion angle $\nu$.

The reason why we introduce the modified frame is that the ordinary Frenet frame behaves discontinuously under deformation when the ordinary curvature angle vanishes at a point. During the turning-over motion of a Kaleidocycle, it goes through such a state at some points, and the above modified frame behaves consistently even under the situation.

Fix a natural number $N$. A discrete space curve $\gamma$ is said to be *closed* of length $N$ if $\gamma_{n+kN} = \gamma_n$ for any $k \in \mathbb{Z}$. Unlike the ordinary Frenet frame, closeness does not imply $\Phi_{n+kN} = \Phi_n$ but they may differ by rotation by $\pi$ around $T_n$. We say $b$ is oriented (resp. anti-oriented) if $b_n = b_{n+N}$ (resp. $b_n = -b_{n+N}$) for all $n$.

We can consider a discrete version of the Darboux form [32, 70], which gives a correspondence between spherical curves and space curves. Given $b : \mathbb{Z} \to S^2$ with $b_n \times b_{n-1} \neq 0$ for all $n$ and $\varepsilon : \mathbb{Z} \to \mathbb{R}_{\geq 0}$, we can associate a discrete space curve satisfying

$$\gamma_0 = 0, \quad \gamma_n = \gamma_{n-1} + \varepsilon_{n-1} \frac{b_n \times b_{n-1}}{|b_n \times b_{n-1}|}, \tag{5.8}$$

which we denote by $\gamma^{b,\varepsilon}$. The curve $\gamma^{b,\varepsilon}$ is closed of length $N$ if

$$\sum_{n=0}^{N-1} \left( \varepsilon_{k+n} \frac{b_{k+n+1} \times b_{k+n}}{|b_{k+n+1} \times b_{k+n}|} \right) = 0 \tag{5.9}$$

for all $k$.

Notice that a serial (resp. closed) hinged network with $\iota_v = 0$ for all $v \in V$ (see Def. 5.4) can be modelled by an open (resp. a closed) discrete space curve; its base points form the curve and hinge directions are identified with $b_n$ (see Figure 10). This is the crucial observation of this chapter.

Now we introduce our main object, *Kaleidocycles*, which are homogeneous closed hinged networks. We model them as constant speed discrete space curves of constant torsion. They are a generalization to a popular paper toy called the Kaleidocycle (see, e.g., [28, 67]). A serial hinged network similar to our Kaleidocycle is proposed in [57].

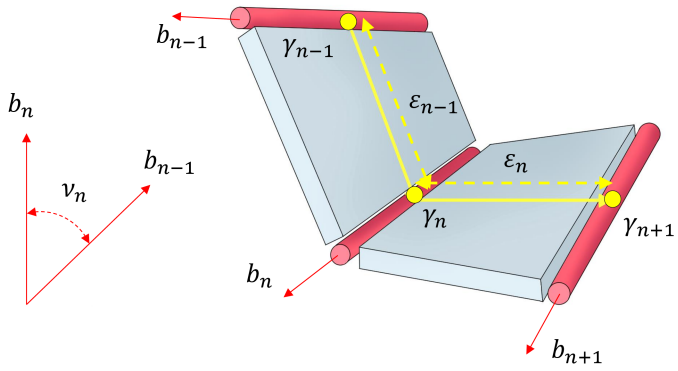


Figure 10: Hinged network and discrete space curve.

**Definition 5.8** *Fix $\nu \in [0,\pi]$ and $\varepsilon > 0$. An $N$-Kaleidocycle with a speed $\varepsilon$ and a torsion angle $\nu$ is a closed discrete space curve $\gamma$ of length $N$ which has a constant speed $\varepsilon_n = \varepsilon$ and a constant torsion angle $\nu_n = \nu$. It is said to be* oriented *(resp.* anti-oriented*) when associated $b$ is oriented (resp. anti-oriented).*

When $\nu$ is either 0 or $\pi$, the corresponding Kaleidocycles are planar, and we call them *degenerate*. For fixed $N$ and $\varepsilon$, an oriented (resp. anti-oriented) non-

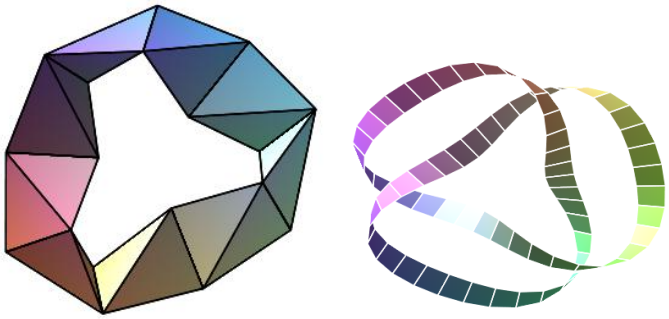

Figure 11: Left: anti-oriented Kaleidocycle with $N = 9$. Right: a Kaleidocycle with a knotted topology.

degenerate Kaleidocycle with a torsion angle $\nu$ is determined by the Darboux form $\gamma^{b,\varepsilon}$ by a map $b : \mathbb{Z} \to S^2$ satisfying p

- $b_{n+N} = b_n$ (resp. $b_{n+N} = -b_n$),
- $\langle b_n, b_{n+1} \rangle = \cos\nu$,
- $\sum_{n=0}^{N-1} b_{n+1} \times b_n = 0$.

We use $b$ and $\gamma$ interchangeably to represent a Kaleidocycle.

Consider the real algebraic variety $\overline{\mathscr{M}_N}$ defined by the following system of quadratic equations ( [68, Ex. 5.2, 8.13]):

$$\langle b_n, b_{n+1}\rangle = c \quad (0 \le n < N), \qquad \sum_{n=0}^{N-1} b_{n+1} \times b_n = 0, \qquad b_N = \pm b_0, \quad (5.10)$$

where $c$ is considered as an indeterminate. The orthogonal group $O(3)$ acts on $b_i$'s in the standard way, and hence, on $\overline{\mathscr{M}_N}$. Denote by $\mathscr{M}_N$ the quotient of $\overline{\mathscr{M}_N}$ by the action of $O(3)$. The variety $\mathscr{M}_N$ serves as the configuration space of all $N$-Kaleidocycles with varying $c = \cos\nu$. It decomposes into two disjoint sub-spaces $\mathscr{M}_N^+$ consisting of all oriented Kaleidocycles ($b_N = b_0$) and $\mathscr{M}_N^-$ consisting of anti-oriented ones ($b_N = -b_0$).

As $\mathscr{M}_N^-$ (resp. $\mathscr{M}_N^+$) is a closed variety, its image under the projection $\pi_c$ onto the $c$-axis is a union of closed intervals. Notice that the image $\pi_c(\mathscr{M}_N^-)$ does not coincide with the whole interval $[-1,1]$; $c = 1$ means $b_i$ are all equal so we cannot have $b_N = -b_0$. The fibre $\pi_c^{-1}(c)$ consists of $N$-Kaleidocycles with a fixed $c$. With a generic value of $c$, a simple dimension counting in (5.10) shows that $\dim(\pi_c^{-1}(c)) = N-6$. Hence, the degree of freedom (DOF) of the Kaleidocycle with a torsion angle $\nu = \arccos(c)$ is generally $N-6$. For $N > 6$, a generic Kaleidocycle is *reconfigurable* meaning that it can continuously change its shape. We will investigate a particular series of reconfiguration in the next section.

**Remark 5.9** *The most popular Kaleidocycle with $N = 6$ has $c = 0$, which is equivalent to the threefold symmetric Bricard 6R linkage (Figure 2). This Kaleidocycle is highly symmetric and not generic, resulting in* 1 *DOF [37].*

## 5.4 Continuous isoperimetric deformations on discrete curves

Kaleidocycles exhibit a characteristic turning-over motion (see Figure 12 and see [46] for some animations). In general, an $N$-Kaleidocycle has $N-6$ degrees of freedom so that it wobbles in addition to turning-over. With special values of torsion angle, however, the DOF of the Kaleidocycle seems to degenerate to exactly one, leaving only the turning-over motion as we will discuss in Section 5.6. In this case, the motion of the core segment looks to be orthogonal to the hinge directions. In the following, we would like to model the motion explicitly. It turns out that we can construct the motion of Kaleidocycles using semi-discrete mKdV and sine-Gordon equations.

In this section, we consider certain continuous deformations of discrete space curves which correspond to motion of homogeneous serial and closed hinged

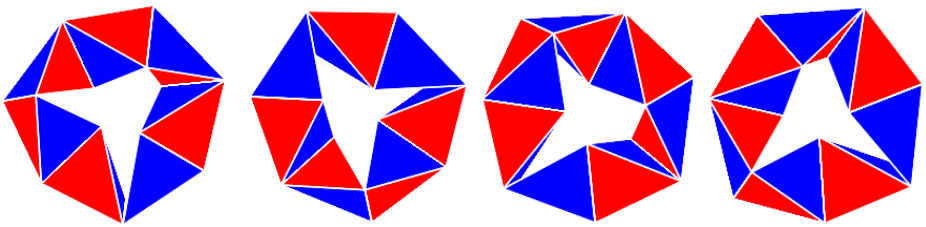

Figure 12: Turning-over motion of a Kaleidocycle with $N = 7$.

networks. Our approach is to construct a flow on the configuration space by differential-difference equations. We use the same notations as in Section 5.3. Observe that a hinged network moves in such a way that its tetrahedral links are not distorted. In the language of discrete space curves, the motion corresponds to a deformation which preserves the speed $\varepsilon_n$ and the torsion angle $\nu_n$ for all $n$.

Let $\gamma(0) : \mathbb{Z} \to \mathbb{R}^3$ be an (open) discrete space curve which has a constant speed $\varepsilon_n(0) = \varepsilon_*(0)$ and a constant torsion angle $\nu_n(0) = \nu_*(0)$. Given a family of functions $w(t) : \mathbb{Z} \to \mathbb{R}$ with the deformation parameter $t \in \mathbb{R}$ and a constant $\rho > 0$, we consider a family of discrete space curves $\gamma(t)$ defined by

$$\frac{d\gamma_n}{dt} = \frac{\varepsilon_n}{\rho}\left(\cos w_n T_n + \sin w_n \widetilde{N}_n\right) \qquad (n \in \mathbb{Z}). \tag{5.11}$$

That is, the motion of each point $\gamma_n$ is confined in the osculating plane and its speed depends only on the length of the segment $\varepsilon_n = |\gamma_{n+1} - \gamma_n|$. We say a deformation is *isoperimetric* if the segment length $\varepsilon_n$ does not depend on $t$ for all $n$, We would like to find conditions on $w$ under which the above deformation is isoperimetric. From (5.2), (5.6) and (5.11), we have

$$\begin{aligned}
\frac{d\varepsilon_n}{dt} &= \frac{\varepsilon_n}{\rho}\left\langle \Phi_{n+1}\begin{bmatrix}\cos w_{n+1}\\ \sin w_{n+1}\\ 0\end{bmatrix} - \Phi_n\begin{bmatrix}\cos w_n\\ \sin w_n\\ 0\end{bmatrix}, \Phi_n\begin{bmatrix}1\\0\\0\end{bmatrix}\right\rangle \\
&= \frac{\varepsilon_n}{\rho}\left\langle \Phi_n\begin{bmatrix}\cos(\kappa_{n+1}+w_{n+1}) - \cos w_n\\ \cos\nu_n \sin(\kappa_{n+1}+w_{n+1}) - \sin w_n\\ -\sin\nu_n \sin(\kappa_{n+1}+w_{n+1})\end{bmatrix}, \Phi_n\begin{bmatrix}1\\0\\0\end{bmatrix}\right\rangle \\
&= \frac{\varepsilon_n}{\rho}\left(\cos(\kappa_{n+1}+w_{n+1}) - \cos w_n\right).
\end{aligned}$$

Therefore, for each $n$, $d\varepsilon_n/dt$ vanishes if and only if

$$\cos(\kappa_{n+1}+w_{n+1}) - \cos w_n = 0, \tag{5.12}$$

which yields

$$w_n = -w_{n-1} - \kappa_n, \tag{5.13}$$

or

$$w_n = w_{n-1} - \kappa_n. \tag{5.14}$$

We consider a deformation when (5.13) (resp. (5.14)) simultaneously holds for all $n$. Note that in this case $w_n(t)$ for all $n$ is determined once $w_0(t)$ is given.

Those deformations are characterized by the following propositions:

**Proposition 5.10** *Let $\gamma(0) : \mathbb{Z} \to \mathbb{R}^3$ be a discrete space curve with a constant speed $\varepsilon_n(0) = \varepsilon_*(0)$ and a constant torsion angle $\nu_n(0) = \nu_*(0)$. Let $\gamma(t)$ be its deformation according to (5.11) with $w : \mathbb{Z} \to \mathbb{R}$ satisfying the condition (5.13). Then we have:*

1. *The speed $\varepsilon_n(t)$ and the torsion angle $\nu_n(t)$ do not depend on $t$ nor $n$. That is, $\varepsilon_n(t) = \varepsilon_*(0)$ and $\nu_n(t) = \nu_*(0)$ for all $t$ and $n$.*

2. *The signed curvature angle $\kappa_n = \kappa_n(t)$ and $w_n = w_n(t)$ satisfy*

$$\frac{d\kappa_n}{dt} = \alpha\left(\sin w_{n-1} - \sin w_n\right), \tag{5.15}$$

*where $\alpha = \frac{1+\cos\nu_*(0)}{\rho}$.*

3. *The deformation of the frame $\Phi_n(t) = [T_n(t), \widetilde{N}_n(t), b_n(t)]$ is given by*

$$\frac{d\Phi_n}{dt} = \Phi_n M_n,$$
$$M_n = \frac{1}{\rho}\begin{bmatrix} 0 & (1+\cos\nu_*(0))\sin w_n & -\sin\nu_*(0)\sin w_n \\ -(1+\cos\nu_*(0))\sin w_n & 0 & \sin\nu_*(0)\cos w_n \\ \sin\nu_*(0)\sin w_n & -\sin\nu_*(0)\cos w_n & 0 \end{bmatrix}. \tag{5.16}$$

**Proposition 5.11** *Let $\gamma(0) : \mathbb{Z} \to \mathbb{R}^3$ be a discrete space curve with a constant speed $\varepsilon_n(0) = \varepsilon_*(0)$ and a constant torsion angle $\nu_n(0) = \nu_*(0)$. Let $\gamma(t)$ be its deformation according to (5.11) with $w : \mathbb{Z} \to \mathbb{R}$ satisfying the condition (5.14). Then we have:*

1. *The speed $\varepsilon_n(t)$ and the torsion angle $\nu_n(t)$ do not depend on $t$ nor $n$. That is, $\varepsilon_n(t) = \varepsilon_*(0)$ and $\nu_n(t) = \nu_*(0)$ for all $t$ and $n$.*

2. *The signed curvature angle* $\kappa_n = \kappa_n(t)$ *and* $w_n = w_n(t)$ *satisfy*

$$\frac{d\kappa_n}{dt} = -\hat{\alpha}\,(\sin w_n + \sin w_{n-1}), \tag{5.17}$$

*where* $\hat{\alpha} = \frac{1-\cos \nu_*(0)}{\rho}$.

3. *The deformation of the frame* $\Phi_n(t) = [T_n(t), \widetilde{N}_n(t), b_n(t)]$ *is given by*

$$\frac{d\Phi_n}{dt} = \Phi_n M_n,$$
$$M_n = \frac{1}{\rho}\begin{bmatrix} 0 & (1-\cos\nu_*(0))\sin w_n & \sin\nu_*(0)\sin w_n \\ -(1-\cos\nu_*(0))\sin w_n & 0 & -\sin\nu_*(0)\cos w_n \\ -\sin\nu_*(0)\sin w_n & \sin\nu_*(0)\cos w_n & 0 \end{bmatrix}. \tag{5.18}$$

*Proof.* We only prove Proposition 5.10 since Proposition 5.11 can be proved in the same manner. We first show the second and the third statements. We denote $\dot{f} = \frac{df}{dt}$, $\nu = \nu_*(0)$ and $\varepsilon = \varepsilon_*(0)$ for simplicity. Since $\varepsilon$ is a constant by the preceding argument, the deformation of $T_n$ can be computed from (5.11) and (5.14) as

$$\begin{aligned} \dot{T}_n &= \frac{1}{\rho}\Phi_n \left( L_n \begin{bmatrix} \cos w_{n+1} \\ \sin w_{n+1} \\ 0 \end{bmatrix} - \begin{bmatrix} \cos w_n \\ \sin w_n \\ 0 \end{bmatrix} \right) \\ &= \frac{1}{\rho}\Phi_n \begin{bmatrix} \cos(\kappa_{n+1}+w_{n+1}) - \cos w_n \\ \cos\nu\sin(\kappa_{n+1}+w_{n+1}) - \sin w_n \\ -\sin\nu\sin(\kappa_{n+1}+w_{n+1}) \end{bmatrix} \\ &= \frac{1}{\rho}\Phi_n \begin{bmatrix} 0 \\ -(1+\cos\nu)\sin w_n \\ \sin\nu\sin w_n \end{bmatrix}. \end{aligned} \tag{5.19}$$

Differentiating $\cos\kappa_n = \langle T_n, T_{n-1}\rangle$ with respect to $t$, we have

$$-\dot{\kappa}_n \sin\kappa_n = \langle \dot{T}_n, T_{n-1}\rangle + \langle T_n, \dot{T}_{n-1}\rangle. \tag{5.20}$$

Noting

$$T_{n-1} = \Phi_n L_{n-1}^{-1}\begin{bmatrix} 1 \\ 0 \\ 0 \end{bmatrix} = \Phi_n \begin{bmatrix} \cos\kappa_n \\ -\sin\kappa_n \\ 0 \end{bmatrix}, \tag{5.21}$$

and

$$\dot{T}_{n-1} = \frac{1}{\rho}\Phi_n L_n^{-1} \begin{bmatrix} 0 \\ -(1+\cos\nu)\sin w_{n-1} \\ \sin\nu \sin w_{n-1} \end{bmatrix} = \frac{1}{\rho}\Phi_n \begin{bmatrix} -(1+\cos\nu)\sin\kappa_n \sin w_{n-1} \\ -(1+\cos\nu)\cos\kappa_n \sin w_{n-1} \\ -\sin\nu \sin w_{n-1} \end{bmatrix}, \tag{5.22}$$

we get from (5.19) and (5.20)

$$\dot{\kappa}_n = \frac{1+\cos\nu}{\rho}\left(\sin w_{n-1} - \sin w_n\right), \tag{5.23}$$

which is equivalent to (5.17). This proves the second statement. Next, we see from the definition of $b_n$

$$\dot{b}_n = \frac{d}{dt}\left(\frac{1}{|T_{n-1}\times T_n|}\right) T_{n-1}\times T_n + \frac{1}{|T_{n-1}\times T_n|}\left(\dot{T}_{n-1}\times T_n + T_{n-1}\times \dot{T}_n\right). \tag{5.24}$$

Noting

$$T_{n-1}\times T_n = \Phi_n \begin{bmatrix} \cos\kappa_n \\ -\sin\kappa_n \\ 0 \end{bmatrix} \times \Phi_n \begin{bmatrix} 1 \\ 0 \\ 0 \end{bmatrix} = \Phi_n \begin{bmatrix} 0 \\ 0 \\ \sin\kappa_n \end{bmatrix}, \tag{5.25}$$

$$\dot{T}_{n-1}\times T_n = \frac{1}{\rho}\Phi_n \begin{bmatrix} -(1+\cos\nu)\sin\kappa_n \sin w_{n-1} \\ -(1+\cos\nu)\cos\kappa_n \sin w_{n-1} \\ -\sin\nu \sin w_{n-1} \end{bmatrix} \times \Phi_n \begin{bmatrix} 1 \\ 0 \\ 0 \end{bmatrix} = \frac{1}{\rho}\Phi_n \begin{bmatrix} 0 \\ -\sin\nu \sin w_{n-1} \\ (1+\cos\nu)\cos\kappa_n \sin w_{n-1} \end{bmatrix}, \tag{5.26}$$

and

$$T_{n-1}\times \dot{T}_n = \Phi_n \begin{bmatrix} \cos\kappa_n \\ -\sin\kappa_n \\ 0 \end{bmatrix} \times \frac{1}{\rho}\Phi_n \begin{bmatrix} 0 \\ -(1+\cos\nu)\sin w_n \\ \sin\nu \sin w_n \end{bmatrix} = \frac{1}{\rho}\Phi_n \begin{bmatrix} -\sin\nu \sin\kappa_n \sin w_n \\ -\sin\nu \cos\kappa_n \sin w_n \\ -(1+\cos\nu)\cos\kappa_n \sin w_n \end{bmatrix}, \tag{5.27}$$

we get from (5.23) and (5.24)

$$\dot{b}_n = \frac{1}{\rho}\Phi_n \begin{bmatrix} -\sin\nu \sin w_n \\ \sin\nu \cos w_n \\ 0 \end{bmatrix}. \tag{5.28}$$

We immediately obtain $\dot{\tilde{N}}_n$ from (5.19) and (5.24) as

$$\dot{\tilde{N}} = \dot{b_n} \times T_n + b_n \times \dot{T_n} = \frac{1}{\rho}\Phi_n \begin{bmatrix} (1+\cos\nu)\sin w_n \\ 0 \\ -\sin\nu\cos w_n \end{bmatrix}. \tag{5.29}$$

Then we have (5.18) from (5.19), (5.24) and (5.29), which proves the third statement. Finally, differentiating $\cos\nu = \langle b_n, b_{n-1}\rangle$ with respect to $t$, it follows from (5.28) and (5.12) that

$$-\dot{\nu}\sin\nu = \langle \dot{b_n}, b_{n-1}\rangle + \langle b_n, \dot{b}_{n-1}\rangle = -\frac{\sin^2\nu}{\rho}\big(\cos(\kappa_n + w_n) - \cos w_{n-1}\big) = 0,$$

which implies $\dot{\nu} = 0$. This completes the proof of the first statement. □

**Remark 5.12** *The condition* (5.13) *suggests the potential function* $\theta_n$ *in Proposition* 5.10 *such that we have*

$$\kappa_n = \frac{\theta_{n+1} - \theta_{n-1}}{2}, \quad w_n = \frac{\theta_n - \theta_{n+1}}{2}. \tag{5.30}$$

*Then,* (5.15) *is rewritten as*

$$\frac{d}{dt}(\theta_{n+1} + \theta_n) = 2\alpha\sin\left(\frac{\theta_{n+1} - \theta_n}{2}\right). \tag{5.31}$$

*To the best of the authors' knowledge, this is a novel form of the semi-discrete potential mKdV equation. In fact, the continuum limit* $\alpha = \frac{2}{\varepsilon}$, $X = \varepsilon n + t$, $T = \frac{\varepsilon^2}{12}t$, $\varepsilon \to 0$ *yields the potential mKdV equation*

$$\theta_T + \frac{1}{2}(\theta_X)^3 + \theta_{XXX} = 0. \tag{5.32}$$

*Similarly, introducing the potential function* $\theta_n$ *in Proposition* 5.11 *such that*

$$\kappa_n = \frac{\theta_{n+1} - \theta_{n-1}}{2}, \quad w_n = -\frac{\theta_{n+1} + \theta_n}{2}, \tag{5.33}$$

*suggested by* (5.14)*, we can rewrite* (5.17) *as*

$$\frac{d}{dt}(\theta_{n+1} - \theta_n) = 2\alpha\sin\left(\frac{\theta_{n+1} + \theta_n}{2}\right), \tag{5.34}$$

*which is nothing but the semi-discrete sine-Gordon equation [27, 63, 64].*

**Remark 5.13** *In the above argument, we assume that the speed of the deformation $\rho$ in (5.11) is a constant and does not depend on $n$. Then, by demanding that the deformation preserve arc length ((5.13) or (5.14)), it followed that the torsion angle is also preserved. Conversely, it seems to be the case that for the deformation to preserve both the arc length and the torsion angle, the speed $\rho$ is required not to depend on $n$.*

**Remark 5.14 (Continuum limit)** *The isoperimetric torsion-preserving discrete deformations for the discrete space curves of constant torsion have been considered in [1], where the deformations are governed by the discrete sine-Gordon and the discrete mKdV equations. It is possible to obtain the continuous deformations discussed in this section by suitable continuum limits from those discrete deformations. More precisely, let $\gamma_n^m$ ($m \in \mathbb{Z}$) be a family of discrete curves obtained by applying the discrete deformations $m$ times to $\gamma_n^0 = \gamma_n$, where $\gamma_n$ is the discrete curve with a constant speed $\varepsilon$ and a constant torsion angle $\nu$. Then the above discrete deformation is given by*

$$\gamma_n^{m+1} = \gamma_n^m + \delta_m \left(\cos w_n^m T_n^m + \sin w_n^m N_n^m\right). \tag{5.35}$$

*Then if we choose $\delta_m$ and $w_0^m$ so that the sign of $\sigma_n^m = \sin\left(w_{n+1}^m + \kappa_{n+1}^m - w_{n-1}^m\right)$ does not depend on $n$, the isoperimetric condition and the compatibility condition of the Frenet frame yield the discrete mKdV equation*

$$\frac{w_{n+1}^{m+1} - w_n^m}{2} = \arctan\left(\frac{b+a}{b-a}\tan\frac{w_n^{m+1}}{2}\right) - \arctan\left(\frac{b+a}{b-a}w_{n+1}^m\right), \tag{5.36}$$

*when $\sigma_n^m > 0$, and the discrete sine-Gordon equation*

$$\frac{w_{n+1}^{m+1} + w_n^m}{2} = \arctan\left(\frac{b+a}{b-a}\tan\frac{w_n^{m+1}}{2}\right) + \arctan\left(\frac{b+a}{b-a}w_{n+1}^m\right), \tag{5.37}$$

*when $\sigma_n^m < 0$ with*

$$a = \left(1 + \tan^2\frac{\nu}{2}\right)\varepsilon, \quad b = \left(1 + \tan^2\frac{\nu}{2}\right)\delta. \tag{5.38}$$

*For the discrete mKdV equation (5.36), in the limit of*

$$a = \frac{2\varepsilon}{\rho\alpha}, \quad m = \frac{\rho}{\varepsilon\delta}t, \quad b \to 0\ (\delta \to 0), \tag{5.39}$$

*(5.36) is reduced to the semi-discrete mKdV equation (5.15). Similarly, the discrete sine-Gordon equation (5.37) is reduced to the semi-discrete sine-Gordon equation (5.17) in the limit*

$$a = \frac{\alpha\rho}{\varepsilon}, \quad m = \frac{\rho}{\varepsilon\delta}t, \quad b \to \infty\ (\delta \to 0). \tag{5.40}$$

*Obviously, the discrete deformation equation of the discrete curve* (5.35) *is reduced to the continuous deformation equation* (5.11)*. Moreover, it is easily verified that the discrete deformation equations of the Frenet frame in [1] are reduced to* (5.16) *and* (5.18)*.*

## 5.5 Turning-over motion of Kaleidocycles

An $N$-Kaleidocycle corresponds to a closed discrete curve $\gamma$ of length $N$ having a constant speed $\varepsilon$ and a constant torsion angle $\nu$ whose $b$ is oriented. Since $\gamma$ is closed, for (5.11) to define a deformation of $\gamma$, we need a periodicity condition $w_{n+N} = w_n$ (when oriented) or $w_{n+N} = -w_n$ (when anti-oriented) for any $n \in \mathbb{Z}$.

When $N$ is odd and the Kaleidocycle is oriented, the equation (5.13) together with $w_0 = w_N$ forms a linear system for $w_n$ $(0 \leq n \leq N)$ which is regular. Therefore, we can find $w_n$ $(0 \leq n \leq N)$ uniquely as the solution to the system. Then, the equation (5.11) generates a deformation of $\gamma$ which preserves the segment length and the torsion angle, while $\gamma$ remains closed. That is, the turning-over motion of the Kaleidocycle is governed by the semi-discrete mKdV equation (5.15) (see Figure 13). Note that by (5.15), the total curvature angle $\sum_{i=0}^{N-1} \kappa_n(t)$ is also preserved.

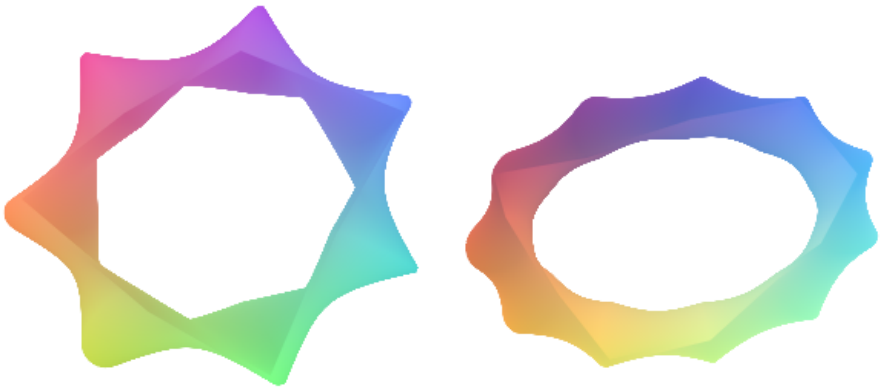

Figure 13: Surface drawn by the evolution of the center curves of Kaleidocycles with $N = 7$ and $N = 25$ respectively.

When the Kaleidocycle is anti-oriented, the equation (5.14) together with $w_0 = -w_N$ forms a linear system for $w_n$ $(0 \leq n \leq N)$ which is regular for any $N$. Similarly to the above, in this case the turning-over motion of the Kaleidocycle is governed by the semi-discrete sine-Gordon equation (5.17).

Note that if an $N$-Kaleidocycle with an odd $N$ is anti-oriented $b_0 = -b_N$, we can define an oriented Kaleidocycle by taking its "mirrored image" $b_i \mapsto (-1)^i b_i$

which conforms to the definition 5.8. Thus, for an odd Kaleidocycle, both the semi-discrete mKdV equation and the semi-discrete sine-Gordon equation generate the turning-over motion.

## 5.6 Extreme Kaleidocycles

We defined Kaleidocycles in Def. 5.8 and saw the torsion angle cannot be chosen arbitrarily. A natural question is for what torsion angle $\nu$ there exists an $N$-Kaleidocycle for each $N$. It seems there are no Kaleidocycles with $\nu \in (0,\pi)$ for $N \leq 5$. For $6 \leq N \leq 50$, we conducted numerical experiments with [46] and found that there exists $c_N^* \in [0,1]$ which satisfy the following. Recall that $\pi_c : \mathscr{M}_N \to \mathbb{R}$ is the projection of the configuration space $\mathscr{M}_N$ onto the $c$-axis, where $c = \cos\nu$.

1. When $N$ is odd, $\pi_c(\mathscr{M}_N^+) = [-c_N^*, 1]$ and $\pi_c(\mathscr{M}_N^-) = [-1, c_N^*]$.
2. When $N$ is even, $\pi_c(\mathscr{M}_N^+) = [-1, 1]$ and $\pi_c(\mathscr{M}_N^-) = [-c_N^*, c_N^*]$.

Moreover, $N\arccos(c_N^*)$ converges monotonously to a constant, where arccos takes the principal value in $[0,\pi]$. Interestingly, at the boundary values $c = \pm c_N^*$, the fibre of $\pi_c$ seems to be exactly one-dimensional for any $N \geq 6$. This means, they are exactly the one-dimensional orbits defined in Section 5.5.

We summarize our numerical findings.

**Conjecture 5.1** *Let $N \geq 6$. We have the following:*

1. *The space $\pi_c^{-1}(c_N^*) \cap \mathscr{M}_N^-$ is a circle. Moreover, the involution defined by $b_n \mapsto (-1)^n b_n$ induces isomorphisms $\pi_c^{-1}(-c_N^*) \cap \mathscr{M}_N^+ \simeq \pi_c^{-1}(c_N^*) \cap \mathscr{M}_N^-$ when $N$ is odd and $\pi_c^{-1}(-c_N^*) \cap \mathscr{M}_N^- \simeq \pi_c^{-1}(c_N^*) \cap \mathscr{M}_N^-$ when $N$ is even.*
2. *The orbit of any element $\gamma \in \pi_c^{-1}(c_N^*) \cap \mathscr{M}_N^-$ of the flow generated by the semi-discrete sine-Gordon equation described in Section 5.5 coincides with $\pi_c^{-1}(c_N^*) \cap \mathscr{M}_N^- \simeq S^1$.*
3. *When $N$ is odd, the orbit of any element $\gamma \in \pi_c^{-1}(-c_N^*) \cap \mathscr{M}_N^+$ generated by the semi-discrete mKdV equation described in Section 5.5 coincides with $\pi_c^{-1}(-c_N^*) \cap \mathscr{M}_N^+ \simeq S^1$. Moreover, on $\pi_c^{-1}(-c_N^*) \cap \mathscr{M}_N^+$ we have $\sum_{n=0}^{N-1} \kappa_n = 0$ and we can also define its deformation by the semi-discrete sine-Gordon equation if we define $w$ by (5.14) and $\sum_{n=0}^{N-1} \dot{\kappa}_n = 2\alpha \sum_{n=0}^{N-1} \sin(w_n) = 0$. The orbit coincides with $\pi_c^{-1}(-c_N^*) \cap \mathscr{M}_N^+$ as well. That is, for an oriented Kaleidocycle with $\nu = \arccos(-c_N^*)$, we can define two motions one by the semi-discrete sine-Gordon equation (5.14), the other by the semi-discrete mKdV equation (5.13), and they coincide up to rigid transformations.*

4. *Any strip* $(\gamma^{b,\varepsilon}, b)$ *corresponding to* $b \in \pi_c^{-1}(c_N^*) \cap \mathscr{M}_N^-$ *is a 3-half twisted Möbius strip (see Section 5.8). There are no Kaleidocycles with one or two half twisting.*

5. *When N tends to infinity,* $N \arccos c_N^*$ *converges to a constant. There exists a unique limit curve up to congruence for any sequence* $\gamma_N \in \pi_c^{-1}(c_N^*) \cap \mathscr{M}_N^-$*, and it has a constant torsion up to sign.*

We call those Kaleidocycles having the extremal torsion angle *extreme Kaleidocycles*.

**Remark 5.15** *The extreme Kaleidocycles were discovered by the first named author and his collaborators [45, 47]. In particular, when it is anti-oriented, it is called the* Möbius Kaleidocycle *because they are a discrete version of the Möbius strip with a* $3\pi$*-twist. Coincidentally, Möbius is the first one to give the dimension counting formula for generic linkages [56] (although it is often attributed to Maxwell), and our Möbius Kaleidocycles are exceptions to his formula.*

We end this chapter with a list of interesting properties, questions and some supplementary materials of Kaleidocycles for future research.

## 5.7 Kinematic energy

Curves with adapted frames serve as a model of elastic rods and are studied, for example, in Langer and Singer [53] in a continuous setting, and in [26] in a discrete setting. Serial and closed hinged networks are discrete curves with specific frames as we saw in Section 5.3. From this viewpoint, we consider some energy functionals defined for discrete curves with frames and investigate how they behave on the configuration space $\mathscr{M}_N$ of Kaleidocycles.

Let $\gamma$ be a constant speed discrete closed curve of length $N$. The *elastic energy* $\mathscr{E}_e$ and the *twisting energy* $\mathscr{E}_t$ are defined respectively by

$$\mathscr{E}_e(\gamma) = \sum_{n=0}^{N-1} \kappa_n^2, \qquad \mathscr{E}_t(\gamma) = \sum_{n=0}^{N-1} \nu_n^2.$$

By the definition of Kaleidocycle, $\mathscr{E}_t$ takes a constant value when a Kaleidocycle undergoes any motion.

Interestingly, a numerical simulation by [46] suggests that on $\pi_c^{-1}(c_N^*) \cap \mathscr{M}_N^-$ (and also on $\pi_c^{-1}(-c_N^*) \cap \mathscr{M}_N^+$ for an odd $N$ and on $\pi_c^{-1}(-c_N^*) \cap \mathscr{M}_N^-$ for an even $N$) for a fixed $N$, $\mathscr{E}_e$ takes an almost constant value. The summands of $\mathscr{E}_e$ are locally determined and vary depending on the states, however, the total is almost

stable so that only small force should be applied to rotate the Kaleidocycle. It is also noted that the sum $\mathscr{E}_e + \mathscr{E}_t$ is a discrete version of the elastic energy of the Kirchoff rod defined by the strip, and it also takes almost constant values.

Similarly, we introduce the following three more energy functionals, which are observed to take almost constant values on $\pi_c^{-1}(-c_N^*) \cap \mathscr{M}_N^+$. The *dipole energy* is defined to be

$$\mathscr{E}_d(\gamma) := 2\left(\sum_{i<j} \frac{\langle b_i, b_j \rangle}{|\gamma_i - \gamma_j|^3} - 3\frac{\langle b_i, \gamma_i - \gamma_j \rangle \langle b_j, \gamma_i - \gamma_j \rangle}{|\gamma_i - \gamma_j|^5}\right).$$

The *Coulomb energy* with an exponent $\alpha > 0$ is defined to be

$$\mathscr{E}_c(\gamma) := 2\sum_{i<j} \frac{1}{|\gamma_i - \gamma_j|^\alpha}.$$

The *averaged hinge magnitude* is defined to be

$$\mathscr{E}_a(\gamma) := \frac{1}{N}\left|\sum_{n=0}^{N-1} b_n\right|.$$

However, we have no rigorous statements about them. It may be the case that one needs some other discretization of the continuous counterparts of these energies to show their behavior theoretically. It is also interesting to characterize or generalize extreme Kaleidocycles in terms of variational calculus on the space of discrete closed curves.

## 5.8 Topological invariants

As noted in [53], for a curve to be closed, topological constraints come into the story. This quantises some continuous quantity and makes it an isotopy invariant.

Let $\gamma$ be a constant speed discrete closed curve of length $N$. First, interpolate $\gamma_n$ and $b_n$ for $(0 \leq n < 2N)$ linearly to obtain a continuous vector field $\bar{b}$ defined on the polygonal curve $\bar{\gamma}$, which goes around the polygon twice. We define the *twisting number* $\mathscr{T}$ of $\gamma$ as the linking number between twice the centre curve $\bar{\gamma}$ and the boundary curve $\bar{\gamma} + \varepsilon\bar{b}$, where $\varepsilon > 0$ is small enough. Intuitively, it is the number of half-twists of the strip defined by $\gamma$ and $b$. The Călugăreanu-White formula relates this topological invariant to the sum of two conformal invariants and provides a direct discretization without the need of interpolation (cf. [50]):

$$\mathscr{T} = 2(Tw + Wr), \tag{5.41}$$

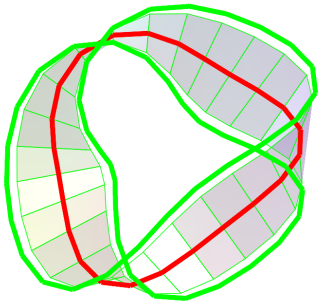

Figure 14: Twisting number as the linking number between centre and boundary curves.

where $Wr$ is the *writhe* of the polygonal curve $\gamma$ which can be computed as a double summation [50, Eq. (13)] and

$$Tw = \frac{1}{2\pi} \sum_{n=0}^{N-1} \nu$$

is the *total twist*. The twisting number $\mathscr{T}$ takes values in the integers, enforcing topological constraints to the curve.

Recall by definition that anti-oriented extreme Kaleidocycles are discrete closed space curves of constant speed and constant torsion which have the minimum odd twisting number. Our numerical experiments suggest that the minimum is not one but three.

Let $\gamma$ be a discrete closed space curve of constant speed and constant torsion corresponding to a Kaleidocycle. Under any motion of the Kaleidocycle, $Tw$ stays constant by definition. By (5.41) the corresponding deformation of the curve preserves the writhe as well. This can equivalently be phrased in terms of the *Gauss map* $G(\gamma) : n \mapsto T_n$ $(0 \leq n \leq N-1)$. The Gauss-Bonnet theorem tells us that $A + 2\pi Tw = 0 \mod \pi$, where $A$ is the area on the sphere enclosed by $G(\gamma)$. By (5.41) we have $Wr = A/2\pi \mod 1/2$. Thus, the deformation of the closed discrete space curve considered in Section 5.5 induces one of the closed discrete spherical curves which preserves the enclosed area $A$.

Kaleidocycles can be folded from a piece of paper. We include a development plan for the extreme Kaleidocycle with $N = 8$ so that the readers can personally make and investigate its motion.

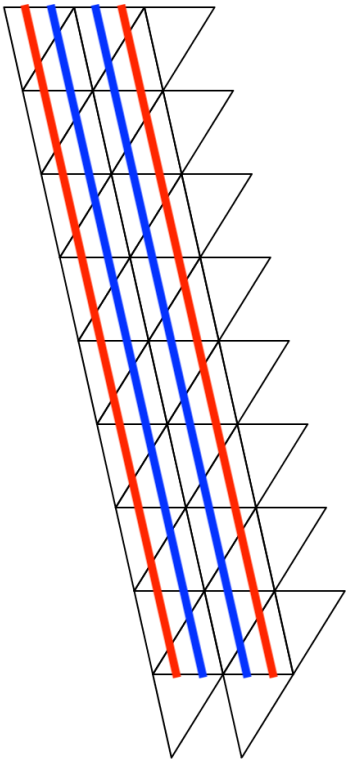

Figure 15: Development plan of an extreme Kaleidocycle with eight hinges. Black horizontal lines indicate valley folds and black slanted lines indicate mountain folds.

# 6 Spherical Kaleidocycles

In this chapter, we introduce a figure on 3-sphere $\left(\mathbb{S}^3\right)$ in $\mathbb{R}^4$, which is called the *spherical Kaleidocycle*. That is a circular chain of linked geodesic tetrahedra on $\mathbb{S}^3$, where all vertices are lied on a Clifford torus, and it turns-over into a periodic motion by $\mathbb{S}^3$-isometries. Then, after it is stereographic projected into $\mathbb{R}^3$, the chain deforms conformally by the corresponding global conformal motion in $\mathbb{R}^3$. This motion of spherical Kaleidocycles looks similar as the turning-over motion of Kaleidocycles, which we considered in Chapter 5. However, while the motion of Kaleidocyles is local isometric in $\mathbb{R}^3$, the motion of spheical Kaleidocycles is conformal but not isometric in $\mathbb{R}^3$. Thus, they have quite different mathematical properties. We present an algorithm to construct the spherical Kaleidocycles, and introduce properties of them.

## 6.1 Standard unit 3-sphere and Clifford torus

In this section, we briefly review basic theories about 3-sphere and the Clifford torus, which are background theories of the structure of the spherical Kaleidocycles.

The standard unit 3-sphere, denoted by $\mathbb{S}^3$, is the set of points in $\mathbb{R}^4$ defined by

$$\mathbb{S}^3 = \left\{ \begin{pmatrix} x_1 \\ x_2 \\ x_3 \\ x_4 \end{pmatrix} \in \mathbb{R}^4 \ : \ x_1^2 + x_2^2 + x_3^2 + x_4^2 = 1 \right\}. \tag{6.1}$$

Sometimes, it is convenient to regard $\mathbb{S}^3$ as a subset of the space with 2 complex dimensions $\mathbb{C}^2$. In this case, $\mathbb{S}^3$ is given by

$$\mathbb{S}^3 = \left\{ \begin{pmatrix} z_1 \\ z_2 \end{pmatrix} \in \mathbb{C}^2 \ : \ |z_1|^2 + |z_2|^2 = 1 \right\}. \tag{6.2}$$

Now we consider $\mathbb{S}^3$ as the set of 2-dimensional complex numbers in (6.2). Then we can parametrize $\mathbb{S}^3$ with three independent parameters since $\mathbb{S}^3$ is a 3-manifold. Particularly, we consider a function $F : [0, 2\pi) \times [0, 2\pi) \times \left(0, \frac{\pi}{2}\right) \to \mathbb{S}^3$ defined by

$$F(\xi_1, \xi_2, \eta) = \begin{pmatrix} z_1(\xi_1, \xi_2, \eta) \\ z_2(\xi_1, \xi_2, \eta) \end{pmatrix} = \begin{pmatrix} \cos\eta \, e^{\sqrt{-1}(\xi_1 + \xi_2)} \\ \sin\eta \, e^{\sqrt{-1}(\xi_1 - \xi_2)} \end{pmatrix}. \tag{6.3}$$

Then the coordinates of $\mathbb{S}^3$ by $F$ are called the *Hopf coordinates*. For any fixed $\eta$, the function $F$ draws a 2-dimensional torus called the *Clifford torus*, via a stereographic projection $s : \mathbb{R}^4 \to \mathbb{R}^3$ given by

$$s \begin{pmatrix} x_1 \\ x_2 \\ x_3 \\ x_4 \end{pmatrix} := \begin{pmatrix} \hat{x}_1 \\ \hat{x}_2 \\ \hat{x}_3 \end{pmatrix} = \left( \frac{x_1}{1 - x_4}; \frac{x_2}{1 - x_4}; \frac{x_3}{1 - x_4} \right), \tag{6.4}$$

where $z_1 = x_1 + \sqrt{-1}x_2$ and $z_2 = x_3 + \sqrt{-1}x_4$.

**Remark 6.1** *We observe how do parameters $\xi_1$ and $\xi_2$ act on the Clifford torus for fixed $\eta$. We introduce different coordinates of $\mathbb{S}^3$, just for comparison, by a function $F' : [0, 2\pi) \times [0, 2\pi) \times \left(0, \frac{\pi}{2}\right) \to \mathbb{S}^3$ as*

$$F'(\xi_1', \xi_2', \eta') \mapsto \begin{pmatrix} z_1(\xi_1', \xi_2', \eta') \\ z_2(\xi_1', \xi_2', \eta') \end{pmatrix} = \begin{pmatrix} \cos\eta' \, e^{\sqrt{-1}\xi_1'} \\ \sin\eta' \, e^{\sqrt{-1}\xi_2'} \end{pmatrix}. \tag{6.5}$$

*Then, for fixed $\eta = \eta'$, we can see how do parameters $\xi_1$ and $\xi_2$ in (6.3) and $\xi_1'$ and $\xi_2'$ in (6.5) act on a torus, respectively, in Figure 16.*

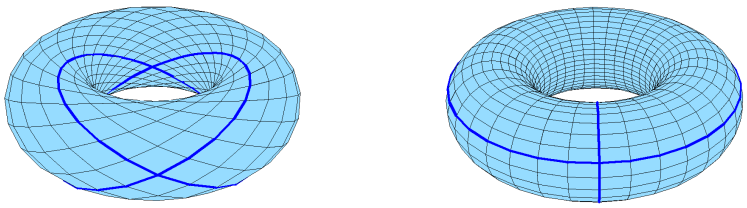

(a) (b)

Figure 16: Profiles of tori(stereographically projected to $\mathbb{R}^3$) by formula (a) in (6.3), (b) and in (6.5), where $\eta = \eta' = \frac{\pi}{6}$.

**Remark 6.2** *The parameter $\eta$ in (6.3) affects the shape of the Clifford torus. We can verify shapes of the Clifford torus when we shall give a value of $\eta$ from 0 to $\pi/2$ in Figure 17.*

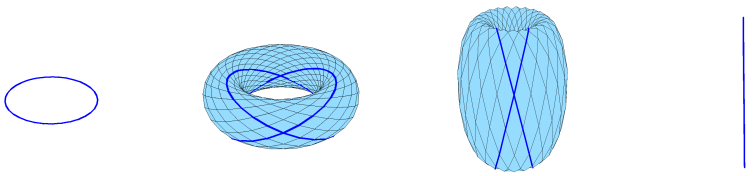

(a) (b) (c) (d)

Figure 17: Profiles of tori by formula in (6.3) with (a) $\eta \to 0$ (b) $\eta = \frac{\pi}{6}$ (c) $\eta = \frac{2\pi}{5}$ (d) $\eta \to \frac{\pi}{2}$.

One interesting way to observe the Clifford torus is to see rotations of the Clifford torus on $\mathbb{S}^3$. It might be not so interesting to consider global rotations of the Clifford torus in $\mathbb{R}^4$. However, if we observe rotations of them in $\mathbb{R}^3$ via a stereographic projection, we can see various moves of the Clifford torus. For example, rotating the Clifford torus on $x_1x_4$-plane in $\mathbb{R}^4$, we get the *Dupin cyclide* via a stereographic projection(see Figure 18). Now we mainly interested in the rotation of the Clifford torus on $x_3x_4$-plane, which is expressed as

$$F(\xi_1, \xi_2, \eta; t) = \begin{pmatrix} \cos\eta\, e^{\sqrt{-1}(\xi_1+\xi_2)} \\ \sin\eta\, e^{\sqrt{-1}(\xi_1-\xi_2+t)} \end{pmatrix}, \tag{6.6}$$

for a real value parameter $t \in \mathbb{R}$. Instead the rotation (6.6) does not give a dramatic change of shape of the Clifford torus, it gives the turning-over motion of

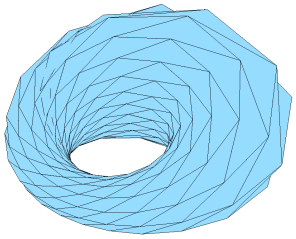

Figure 18: Dupin cyclide, which is derived by rotating the Clifford torus.

the Clifford torus via a stereographic projection(see Figure 19). This turning-over motion looks like the turning-over motion of Kaleidocycles described in Section 5.

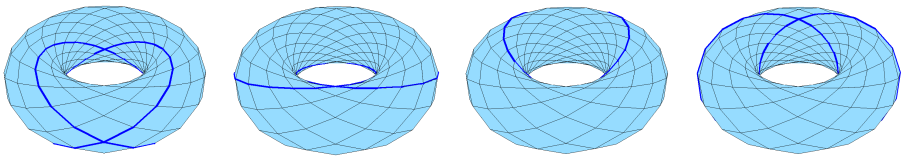

(a) (b) (c) (d)

Figure 19: Profiles of the rotaion of the torus described in (6.6), where (a) $t = 0$ (b) $t = \frac{\pi}{2}$ (c) $t = \pi$ (d) $t = \frac{3\pi}{2}$.

## 6.2 Construction of spherical Kaleidocycles

In this section, we present an algorithm to construct the spherical Kaleidocycles. As a first step, we construct a spherical tetrahedron on $\mathbb{S}^3$, whose segments are parts of some geodesics of $\mathbb{S}^3$. We denote the $x_i x_j$-axis geodesic curve of $\mathbb{S}^3$ by

$$\gamma_{ij} : [-\pi, \pi) \to \mathbb{S}^3, \quad t \mapsto \gamma_{ij}(t), \tag{6.7}$$

and we introduce a notation

$$\gamma_{ij}^{\alpha} := \gamma_{ij}|_{[-\alpha,\alpha]}, \quad \alpha \in (-\pi, \pi). \tag{6.8}$$

Now we put $\gamma_{14} = \gamma_{14}(t)$, and the rotation matrix $R_{14} = R_{14}(\theta) : [0, 2\pi) \to M_{4\times 4}(\mathbb{R})$ as

$$\gamma_{14} = \begin{pmatrix} \sin t \\ 0 \\ 0 \\ \cos t \end{pmatrix}, \quad R_{14} = \begin{pmatrix} \cos\theta & 0 & 0 & \sin\theta \\ 0 & 1 & 0 & 0 \\ 0 & 0 & 1 & 0 \\ -\sin\theta & 0 & 0 & \cos\theta \end{pmatrix}, \tag{6.9}$$

respectively, and we define a spherical segment $H_0 : [-\phi, \phi] \to \mathbb{S}^3$ by

$$H_0 = R_{14}\left(\frac{\pi}{2}\right)\gamma_{14}^{\phi}, \tag{6.10}$$

for some $\phi \in (-\pi, \pi)$. Then denoting the center point of $H_0$ as $P_0$, we have $s \circ P_0 = s \circ H_0(0) = (1,0,0)$, where a function $s$ is the stereographic projection given in (6.4) (see Figure 20).

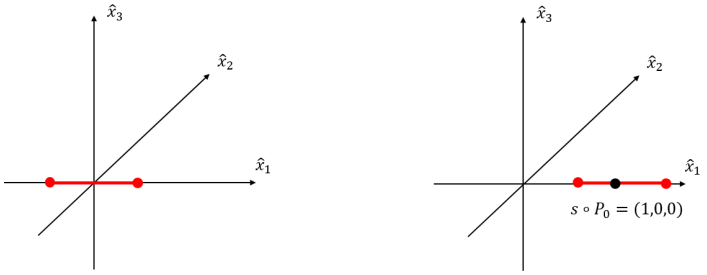


(a) (b)

Figure 20: Profiles of (a) $s \circ \gamma_{14}^{\phi}$ and (b) $s \circ H_0 = s \circ R_{14}(\frac{\pi}{2})\gamma_{14}^{\phi}$.

Now we define an another spherical segment $H_1 : [-\phi, \phi] \to \mathbb{S}^3$ by

$$H_1 = R_{12}\left(\frac{2\pi}{N}\right) R_{14}\left(\frac{\pi}{2}\right) R_{13}(\psi)\, \gamma_{14}^{\phi}, \tag{6.11}$$

for a real number $\psi \in (0, 2\pi)$, and an integer $N \geq 3$(see Figure 21). Here, $R_{12} = R_{12}(\theta)$ and $R_{13} = R_{13}(\theta)$ are rotation matrices defined by

$$R_{12} = \begin{pmatrix} \cos\theta & -\sin\theta & 0 & 0 \\ \sin\theta & \cos\theta & 0 & 0 \\ 0 & 0 & 1 & 0 \\ 0 & 0 & 0 & 1 \end{pmatrix}, \quad R_{13} = \begin{pmatrix} \cos\theta & 0 & -\sin\theta & 0 \\ 0 & 1 & 0 & 0 \\ \sin\theta & 0 & \cos\theta & 0 \\ 0 & 0 & 0 & 1 \end{pmatrix}, \tag{6.12}$$

respectively.

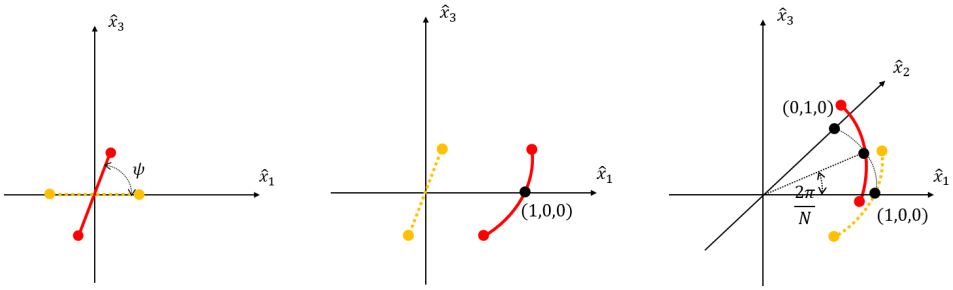


(a) (b) (c)

Figure 21: The red curve in each figure describes (a) $s \circ R_{13}(\psi)\gamma_{14}^{\phi}$, (b) $s \circ R_{14}\left(\frac{\pi}{2}\right)R_{13}(\psi)\gamma_{14}^{\phi}$ and (c) $s \circ R_{12}\left(\frac{2\pi}{N}\right)R_{14}\left(\frac{\pi}{2}\right)R_{13}(\psi)\gamma_{14}^{\phi}$, respectively.

Then now we can construct a spherical tetrahedron on $\mathbb{S}^3$ by putting segments between all of end points of $H_0$ and $H_1$ each other, where we always choose the shortest path on $\mathbb{S}^3$ when we connect two points among them. In Figure 22, we describe a tetrahedron in $\mathbb{R}^3$ by connecting end points of $s \circ H_0$ and $s \circ H_1$ each other. Note that since all of segments of a tetrahedron in Figure 22 are generated after $H_0$ and $H_1$ are projected to $\mathbb{R}^3$, they do not reflect the real shape of segments of spherical tetrahedron on $\mathbb{S}^3$.

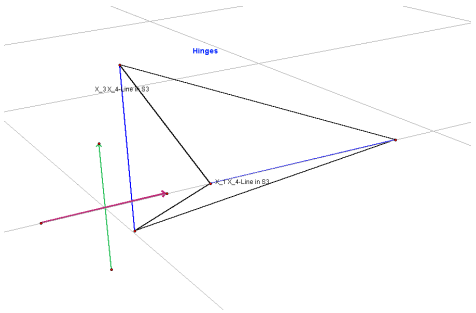


(a)

Figure 22: Profiles of a tetrahedron which is generated by connecting all of end points of $s \circ H_0$ and $s \circ H_1$ each other, where $N = 6$, $\phi = \frac{\pi}{6}$ and $\psi = \frac{\pi}{2}$. Here blue lines describe the $s \circ H_0$ and $s \circ H_1$. Also the red and green arrows describe the $\hat{x}_1$ axis, and the $\hat{x}_3$ axis, respectively.

Let us recall the rotation of the Clifford torus described in (6.6). Now we consider a similar motion of the spherical tetrahedron described in Figure 22. We introduce a family of tetrahedra which are determined by connecting all of end

points of $s \circ R_{34}(t)H_0$ and $s \circ R_{34}(t)H_1$ for each $t \in \mathbb{R}$, where $R_{34} = R_{34}(\theta)$ is the rotation matrix defined by

$$R_{34} = \begin{pmatrix} 1 & 0 & 0 & 0 \\ 0 & 1 & 0 & 0 \\ 0 & 0 & \cos\theta & -\sin\theta \\ 0 & 0 & \sin\theta & \cos\theta \end{pmatrix}. \tag{6.13}$$

Note that it is nothing but the rotation of a spherical tetrahedron on $x_3x_4$-plane. Then we can see the motion of the tetrahedron in Figure 23.

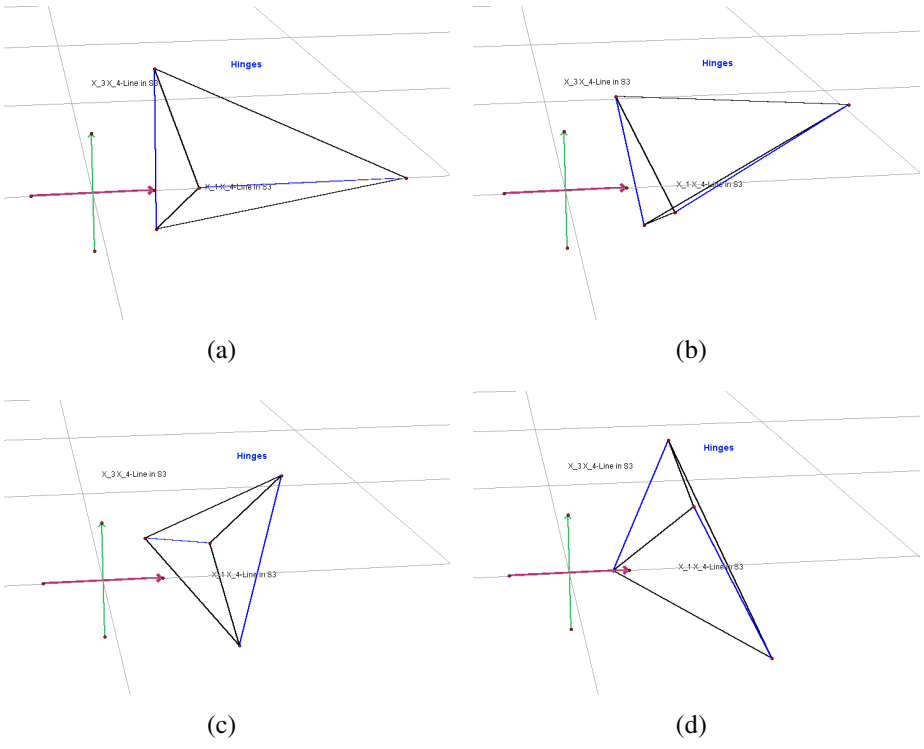


(a) (b) (c) (d)

Figure 23: Rotation on $x_3x_4$-plane of the tetrahedron described in Figure 22. It turns over according to figures (a) $\to$ (b) $\to$ (c) $\to$ (d) $\to$ (a).

Then now we construct a ring of spherical tetrahedra by putting additional spherical segments appropriately: For a real number $\phi \in (-\pi, \pi)$, and an integer $N \geq 3$, we define a series of spherical segments $H_i : [-\phi, \phi] \to \mathbb{S}^3$ by

$$H_i = R_{12}\left(\frac{2i\pi}{N}\right) R_{14}\left(\frac{\pi}{2}\right) R_{13}(i\psi)\, \gamma_{14}^{\phi}. \tag{6.14}$$

Here we choose an angle $\psi \in \mathbb{R}$ such as $N\psi = k\pi$ for an integer $k$ so that $H_i = H_{i+N}$ for all $i$. Then generating $N$ spherical tetrahedra by connecting endpoints of

$H_i$ and $H_{i+1}$ each other for all $i$, we get a closed ring of $N$ spherical tetrahedra, which is called the *spherical Kaleidocycle*(see Figure 24). Note that since each $H_i$ is a common segment of two connected spherical tetrahedra, each $H_i$ plays a similar role as a hinge of Kaleidocycles. For this reason, we call a spherical segment $H_i$ the hinge of spherical Kaleidocycles.

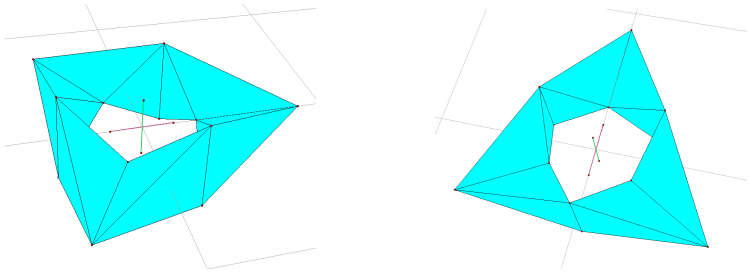

(a) (b)

Figure 24: Profile of the spherical Kaleidocycle, whose hinges are given by (6.14) with same parameters as that in Figure 22, 23.

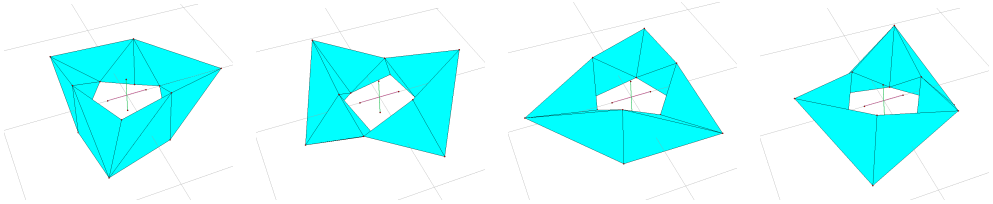

(a) (b) (c) (d)

Figure 25: Rotation on $x_3x_4$-plane of the spherical Kaleidocycle described in Figure 24. It turns over according to figures (a) $\to$ (b) $\to$ (c) $\to$ (d) $\to$ (a).

As we mentioned in Section 6.1, all of segments of the spherical Kaleidocycle in Figure 24 are straight lines since we generated them after every hinge is projected to $\mathbb{R}^3$. If we, however, make them on $\mathbb{S}^3$, all of segments are curved along the face of $\mathbb{S}^3$. To visualize the real form of a spherical Kaleidocycle approximatively, we divide all of faces of a spherical Kaleidocycle, by putting more points on faces, and project all of points to $\mathbb{R}^3$. Then we get a spherical Kaleidocycle whose shapes are close to the real form of that(see Figure 26).

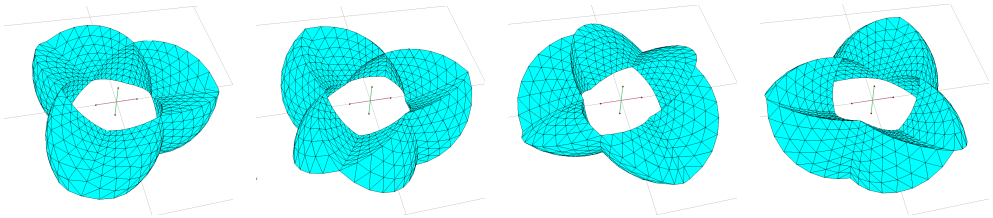

(a) (b) (c) (d)

Figure 26: Rotation on $x_3x_4$-plane of the spherical-Kaleidocycle described in Figure 24, where each face of tetrahedra is divided in 64 triangles It turns over according to figures (a) $\to$ (b) $\to$ (c) $\to$ (d) $\to$ (a).

## 6.3 Gallery

In this section, we present various kind of spherical Kaleidocycles. Unlike Kaleidocycles, spherical Kaleidocycles have various shape up to values of parameters. Though they usually have similar shapes as Kaleidocycles(see Figure 27), they sometimes look like the Möbius strip(see Figure 29). Moreover, if we put the value of the parameter $\phi$ as bigger than $\pi/2$, corresponding spherical Kaleidocycles have the unusual from(see Figure 31).

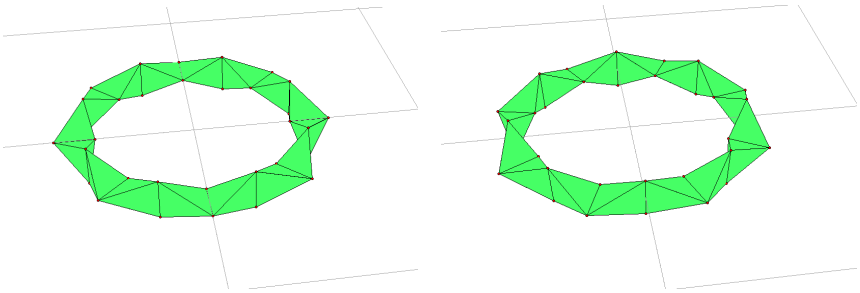

(a) (b)

Figure 27: Spherical Kaleidocycle where $N = 16$, $\phi = \frac{\pi}{18}$ and $\psi = \frac{\pi}{2}$.

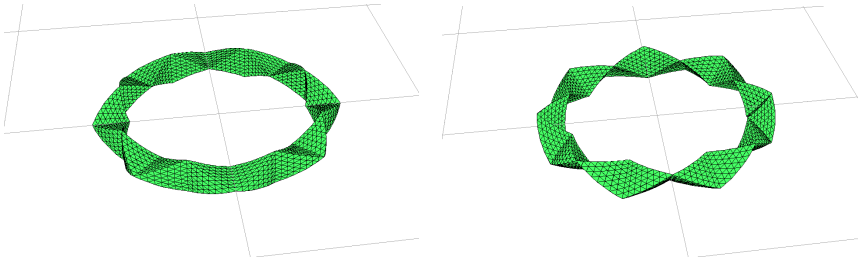

(a) (b)

Figure 28: Spherical Kaleidocycle where $N = 16$, $\phi = \frac{\pi}{18}$ and $\psi = \frac{\pi}{2}$, and each face is divided into 64 triangles.

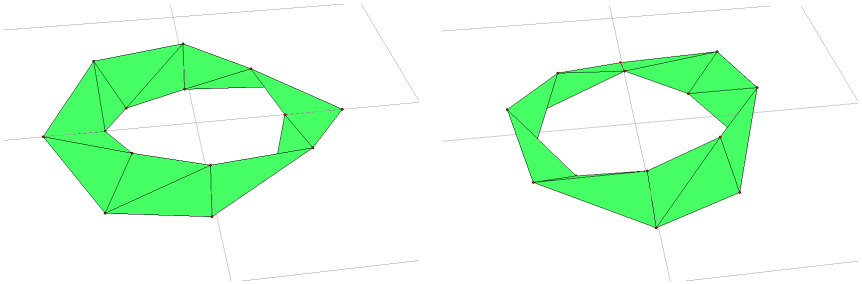

(a) (b)

Figure 29: Spherical Kaleidocycle where $N = 8$, $\phi = \frac{\pi}{6}$ and $\psi = \frac{\pi}{4}$.

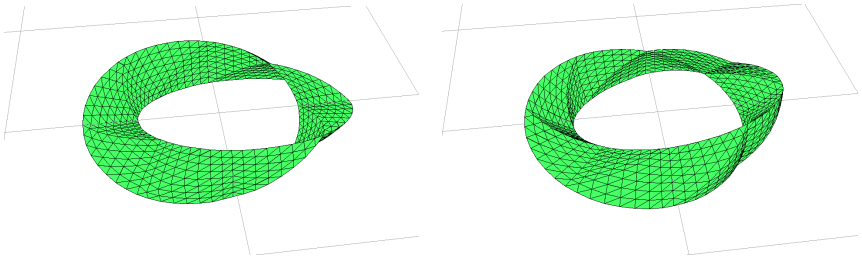

(a) (b)

Figure 30: Spherical Kaleidocycle where $N = 8$, $\phi = \frac{\pi}{6}$ and $\psi = \frac{\pi}{4}$, and each face is divided into 64 triangles.

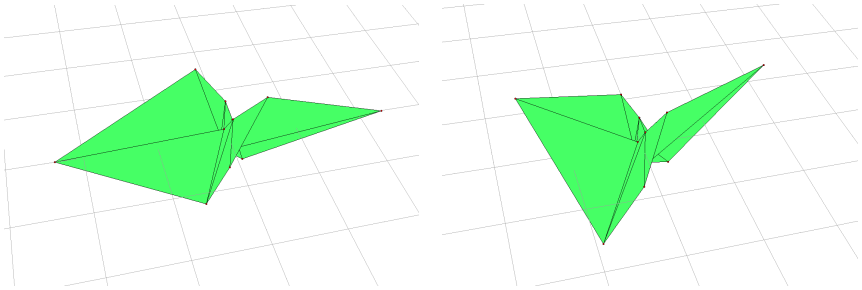

(a) (b)

Figure 31: Spherical Kaleidocycle where $N = 8$, $\phi = \frac{11\pi}{8}$ and $\psi = \frac{\pi}{4}$.

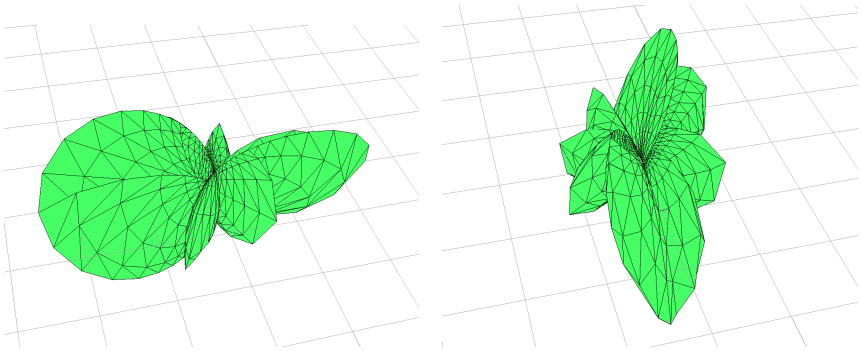

(a) (b)

Figure 32: Spherical Kaleidocycle where $N = 8$, $\phi = \frac{11\pi}{8}$ and $\psi = \frac{\pi}{4}$, and each face is divided into 64 triangles.

# References


[1] J. Inoguchi, K. Kajiwara, N. Matsuura and Y. Ohta, *Discrete mKdV and discrete sine-Gordon flows on discrete space curves*, J. Phys. A: Math. Theor. **47** (2014), 235202.

[2] H. Furuhata, *Surfaces in centroaffine geometry*, RIMS kokyuroku, **1623** (2009), 1–11.

[3] H. Park, K. Kajiwara, T. Kurose and N. Matsuura, *Defocusing mKdV flow on centroaffine plane curves*, JSIAM Lett. **10** (2018), 25–28.

[4] K. -S. Chou and C. Qu, *Integrable equations arising from motions of plane cuves*, Phys. D., **162** (2002), 9–33.

[5] H. Park, *Explicit Formulas for Integrable Deformations of Plane Curves in Various Geometries*, Master's thesis, Kyushu University, 2018.

[6] A. Fujioka and T. Kurose, *Hamiltonian formalism for the higher KdV flows on the space of closed complex equicentroaffine curves*, Int. J. Geom. Methods Mod. Phys. **07** (2010), 165.

[7] U. Pinkall, *Hamiltonian flows on the space of star-shaped curves*, Results Math. **27** (1995), 328–332.

[8] N. Matsuura, *Discrete KdV and discrete modified KdV equations arising from motions of planar discrete curves*, Int. Math. Res. Notices. **2012** (2012), 1681–1698.

[9] C. Rogers and W. K. Schief, *Bäcklund and Darboux Transformations: Geometry and Modern Applications in Soliton Theory*, Cambridge Texts in Applied Mathematics (Cambridge: Cambridge University Press, 2002).

[10] A. I. Bobenko and Y. B. Suris, *Discrete Differential Geometry*, American Mathematics Society, Providence, RI, 2008.

[11] S. Kaji, K. Kajiwara and H. Park *Linkage Mechanisms Governed by Integrable Deformations of Discrete Space Curves, in: Nonlinear Systems and Their Remarkable Mathematical Structure*, Vol. 2, CRC Press, 2019

[12] R. E. Goldstein and D. M. Petrich, *The Korteweg-de Vreis hierarchy as dynamics of closed curves in the plane*, Phys. Rev. Lett. **67** (1991), 3203–3206.

[13] M. Hisakado, K. Nakayama and M. Wadati, *Motion of discrete curves in the plane*, J. Phys. Soc. Jpn. **64** (1995), 2390–2393.

[14] A. Doliwa and P. M. Santini, *The integrable dynamic of a discrete curve, in: Symmetries and Integrability of Difference Equations*, eds. D. Levi, L. Vinet and P. Winternitz, CRM Proceedings and Lecture Notes **9** (Providence: American Mathematical Society, 1996), 91–102.

[15] A. Doliwa and P. M. Santini, *Geometry of discrete curves and lattices and integrable difference equations, in: Discrete Integrable Geometry and Physics*, eds. A. Bobenko and R. Seiler, Oxford Lecture Series in Mathematics and Its Applications **16** (Oxford: Clarendon Press, 1999), 139–154.

[16] U. Pinkall, B. Springborn and S. Weißmann, *A new doubly discrete analogue of smoke ring flow and the real time simulation of fluid flow*, J. Phys. A: Math. Theor. **40** (2007), 12563–12576.

[17] J. Inoguchi, K. Kajiwara, N. Matsuura and Y. Ohta, *Explicit solutions to the semi-discrete modified KdV equation and motion of discrete plane curves*, J. Phys. A: Math. Theor. **45** (2012) 045206.

[18] J. Inoguchi, K. Kajiwara, N. Matsuura and Y. Ohta, *Motion and Bäcklund transformations of discrete plane curves*, Kyushu. J. Math. **66** (2012) 303–324.

[19] S. Hirose, J. Inoguchi, K. Kajiwara, N. Matsuura, Y. Ohta, *Discrete local induction equation*, J. Integrable Syst. **4**(1) (2019), xyz003, 43.

[20] K. -S. Chou and C. -Z. Qu, *Integrable equations arising from motions of plane curves*, Phys. D. **162** (2002), 9–33.

[21] K. -S. Chou and C. -Z. Qu, *Integrable equations arising from motions of plane curves. II*, J. Nonlinear Sci. **13** (2003), 487–517.

[22] K. -S. Chou and C. -Z. Qu, *Motions of curves in similarity geometries and Burgers-mKdV hierarchies*, Chaos Solitons Fractals. **19** (2004), 47–53.

[23] K. Kajiwara, T. Kuroda and N. Matsuura, *Isogonal deformation of discrete plane curves and discrete Burgers hierarchy*, Pac. J. Math. Ind. (2016), 8:3.

[24] R. M. Miura, *Korteweg-de Vries Equation and Generalizations. I. A Remarkable Explicit Nonlinear Transformation*, J. Math. Phys. **9** (1968), 1202–1204.

[25] L. M. Bates and O. M. Melko *On curves of constant torsion I*, J. Geom. **104**(2) (2013), 213–227.

[26] M. Bergou, M. Wardetzky, S. Robinson, B. Audoly and E. Grinspun, *Discrete elastic rods*, ACM Trans. Graph., **27**(3) (2008), Article 63

[27] M. Boiti, F. Pempinelli and B. Prinari, *Integrable discretization of the sine-Gordon equation*, Inverse Problems **18**(5) (2002), 1309–1324.

[28] R. Byrnes, *Metamorphs: Transforming Mathematical Surprises*, Tarquin Pubns, 1999.

[29] A. M. Calini, T. A. Ivey, *Bäcklund transformations and knots of constant torsion*, J. Knot Theory Ram., **7** (1998), 719–746.

[30] A. M. Calini an T. A. Ivey, *Topology and sine-Gordon evolution of constant torsion curves*, Phys. Lett. A, **254**(3–4) (1999), 170–178.

[31] Z. You and Y. Chen, *Motion Structures: Deployable Structural Assemblies of Mechanisms*, Taylor & Francis, 2011.

[32] G. Darboux, *Leçcons sur la Théorie Générale des Surfaces*, Gauthier-Villars, 1917.

[33] J. Denavit and R. S. Hartenberg, *A kinematic notation for lower-pair mechanisms based on matrices*, Trans ASME J. Appl. Mech. **23** (1955), 215–221.

[34] A. Doliwa and P. M. Santini, *An elementary geometric characterization of the integrable motions of a curve*, Phys. Lett. A, **185** (1994), 373–384.

[35] A. Doliwa and P. M. Santini, *Integrable dynamics of a discrete curve and the Ablowitz-Ladik hierarchy*, J. Math. Phys. **36** (1995), 1259–1273.

[36] M. Farber, *Invitation to Topological Robotics*, EMS Zurich, 2008.

[37] P. W. Fowler and S. D. Guest, *A symmetry analysis of mechanisms in rotating rings of tetrahedra*, Proc. R. Soc. A **461** (2005), 1829–1846.

[38] E. C. Freuder, *Synthesizing constraint expressions*, Commun. ACM **21**(11) (1978), 958–966.

[39] H. Hasimoto, *A soliton on a vortex filament*, J. Fluid. Mech. **51** (1972), 477–485.

[40] M. Hisakado and M. Wadati, *Moving discrete curve and geometric phase*, Phys. Lett. A, **214** (1996), 252–258.

[41] T. Hoffmann, *Discrete Differential Geometry of Curves and Surfaces*, MI Lecture Notes vol. 18, Kyushu University, 2009.

[42] R. M. Miura, *Korteweg-de Vries Equation and Generalizations. I. A Remarkable Explicit Nonlinear Transformation*, J. Math. Phys. **9** (1968), 1202–1204.

[43] T. A. Ivey, *Minimal Curves of Constant Torsion*, Proc. AMS, **128**(7) (2000), 2095–2103.

[44] T. Jordán, C. Király and S. Tanigawa, *Generic global rigidity of body-hinge frameworks*, J. Comb. Theory B, **117** (2016), 59–76.

[45] S. Kaji, *A closed linkage mechanism having the shape of a discrete Möbius strip*, the Japan Society for Precision Engineering Spring Meeting Symposium Extended Abstracts, 62–65, 2018. The original is in Japanese but an English translation is available at arXiv:1909.02885.

[46] S. Kaji, *Geometry of the moduli space of a closed linkage: a Maple code*, available at https://github.com/shizuo-kaji/Kaleidocycle

[47] S. Kaji, S. Schönke, M. Grunwald and E. Fried, *Möbius Kaleidocycle*, patent filed, JP2018-033395, 2018.

[48] M. Kapovich and J. Millson, *Universality theorems for configuration spaces of planar linkages*, Topology **41**(6) (2002), 1051–1107.

[49] N. Katoh and S. Tanigawa, *A proof of the molecular conjecture*, Discrete Comput Geom., **45** (2011), 647–700.

[50] K. Klenin and J. Langowski J, *Computation of writhe in modeling of supercoiled DNA*, Biopolymers, **54** (2000), 307–317.

[51] G. L. Lamb Jr., *Solitons and the motion of helical curves*, Phys. Rev. Lett. **37** (1976), 235–237.

[52] J. Langer and R. Perline, *Curve motion inducing modified Korteweg-de Vries systems*, Phys. Lett. A, **239** (1998), 36–40.

[53] J. Langer and D. A. Singer, *Lagrangian aspects of the Kirchhoff elastic rod*, SIAM Review **38**(4) (1996), 605–618.

[54] S. M. LaValle, *Planning algorithms*, Cambridge University Press, 2006.

[55] M. L. S. Magalhães and M. Pollicott, *Geometry and dynamics of planar linkages*, Comm. Math. Phys., **317**(3) (2013), 615–634.

[56] A. F. Möbius, *Lehrbuch der Statik*, **2**, Leipzig, 1837.

[57] M. S. Moses and M. K. Ackerman and G. S. Chirikjian, *ORIGAMI ROTORS: Imparting continuous rotation to a moving platform using compliant flexure hinges*, Proc. IDETC/CIE 2013.

[58] A. Müller, *Representation of the kinematic topology of mechanisms for kinematic analysis*, Mech. Sci., **6** (2015), 1–10.

[59] A. Müller, *Local kinematic analysis of closed-loop linkages – mobility, singularities, and shakiness*, J. Mechanisms Robotics **8**(4) (2016), 041013.

[60] K. Nakayama, *Elementary vortex filament model of the discrete nonlinear Schrödinger equation*, J. Phys. Soc. Jpn. **76** (2007), 074003.

[61] K. Nakayama, H. Segur and M. Wadati, *Integrability and the motions of curves*, Phys. Rev. Lett. **69** (1992), 2603–2606.

[62] K. Nishinari, *A discrete model of an extensible string in three-dimensional space*, J. Appl. Mech. **66** (1999), 695–701.

[63] S. J. Orfanidis S J, *Discrete sine-Gordon equations*, Phys. Rev. D, **18**(10) (1978), 3822–3827.

[64] S. J. Orfanidis, *Sine-Gordon equation and nonlinear $\sigma$ model on a lattice*, Phys. Rev. D, **18**(10) (1978), 3828–3832.

[65] C. Rogers and W. K. Schief, *Bäcklund and Darboux Transformations: Geometry and Modern Applications in Soliton Theory*, Cambridge University Press, Cambridge, 2002.

[66] K. Sato and R. Tanaka, *Solitons in one-dimensional mechanical linkage* Phys. Rev. E, **98** (2018).

[67] D. Schattschneider and W. M. Walker, *M. C. Escher Kaleidocycles*, Pomegranate Communications: Rohnert Park, CA, 1987. (TASCHEN; Reprint edition, 2015).

[68] A. J. Sommese, J. D. Hauenstein, D. J. Bates and C. W. Wampler, *Numerically Solving Polynomial Systems with Bertini*, Software, Environments, and Tools, Vol. 25, SIAM, Philadelphia, PA, 2013.

[69] L. J. Weiner, *Closed curves of constant torsion*, Arch. Math. (Basel) **25** (1974), 313–317.

[70] L. J. Weiner, *Closed curves of constant torsion II*, Proc. AMS, **67**(2) (1977).